Evaporation from Porous Media

Industrial Presenter

W. L. Gore, Inc.

Thirty-Sixth Annual Workshop on Mathematical Problems in Industry
June 14–18, 2020
held virtually; hosted by the University of Vermont

Table of Contents

Introduction

The 36th Annual Workshop on Mathematical Problems in Industry (MPI), was held virtually for the first time from June 14–18, 2020. Participants from multiple time zones across the globe coordinated their efforts to work on the industrial problem presented. Special thanks go to the lead organizer, Taras Lakoba of the University of Vermont, who handled all the hosting and technical duties. Other members of the organizing committee were David A. Edwards and Louis Rossi (University of Delaware), Linda Cummings (New Jersey Institute of Technology), and Richard Moore (Society for Industrial and Applied Mathematics).

At the workshop, several industrial representatives from Gore (Uwe Beuscher, Vasudevan Venkateshwaran, and Zhenyu He) presented the following problem in evaporation in porous media.

In certain liquid filtration problems, a fluid flows through a porous media designed to trap solute molecules. (In the case under consideration, the porous media is polytetrafluoroethylene, better known as PTFE.) As the solvent evaporates, these surfactant molecules are left behind on the internal pore walls. Questions then arise about the mass distribution of the solute molecules left as the solvent evaporates, whether the pores will clog as the evaporation process occurs, etc.

This manuscript is really a collection of reports from teams in the group working on several aspects of the problem. Here is a brief summary of each:

1. Breward *et al.* consider a pore-level analysis. Solute transport and pore clogging are considered for two cases. In the first, the pores are treated as fluid-filled cylinders bounded by the porous media matrix. In the second, the porous media is treated as solid cylinders immersed in the solvent. Analytical and numerical results are obtained, indicating how the pores could clog with solute as the solvent evaporates.
2. Tilley and Broadbridge take a more macroscale approach, considering porous media flow in the filter as a whole. After specifying a suitable dimensionless PDE model, they perform numerical simulations to track the evaporation front and concentration of dissolved surfactant molecules.
3. Gu *et al.* examine the case of two surfactants in water using a ternary diagram and a system of ODEs to track their evolution.

In addition to the authors of these reports, the following people participated in the group discussions:

- Eduardo Corona and Pejman Sanaei, New York Institute of Technology
- Donald Schewendeman, Rensselær Polytechnic Institute
- Naren Vohra, Oregon State University

Pore-Level Analysis

Chris Breward, Kristian Kiradjiev, Attila Kovacs, Maxim Zyskin
Oxford University

Ferran Brosa Planella
University of Warwick

David A. Edwards
University of Delaware

Stefan Llewellyn Smith
University of California, San Diego

David Rumschitzki
City College of New York

Pejman Sanaei
New York Institute of Technology

Yixuan Sun
New Jersey Institute of Technology

Thomas Witelski
Duke University

and others...

August 31, 2020

1 Geometry

In this section we examine the evaporation dynamics in a single pore. We consider the pore to be a cylinder with radius $R_{\rm w}$ (here the subscript "w" stands for "wall") and height H. We begin by tracking the position of the evaporating front $\tilde{h}(\tilde{r},\tilde{t})$ at the top of the evaporating drop.

The advancing contact angle between the filter (which is made of PTFE) and water is greater than $\pi/2$ [19], and the equilibrium one seems to be as well. Therefore, in general $\tilde{h}$ will depend on r. With a contact angle greater than $\pi/2$, the liquid in the pore forms a silo shape (see Fig. 1.1). The top of the silo will just be that portion of a sphere that intersects the pore at the proper angle (a spherical cap), as illustrated in Fig. 1.1. (Note the symmetry in θ.)

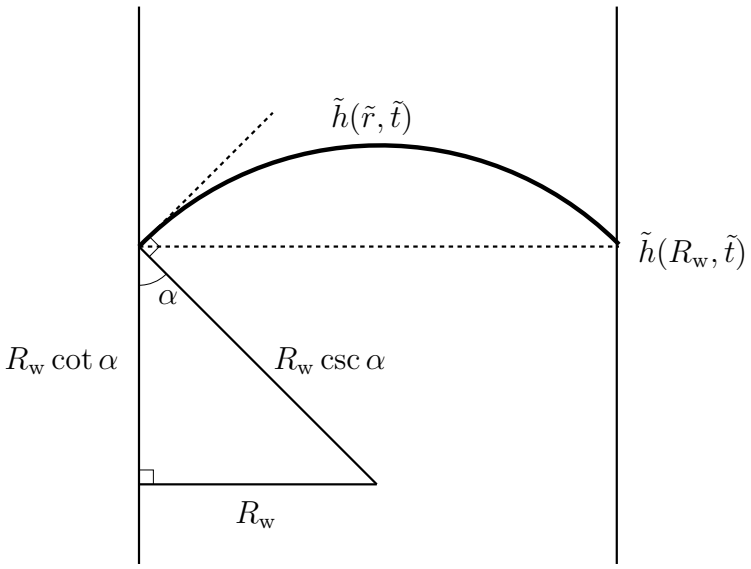

Figure 1.1: Cross-sectional schematic of top of evaporating drop.

If we let the contact angle be $\alpha+\pi/2$, then from Fig. 1.1 the formula for the evaporating front $\tilde{h}(\tilde{r},\tilde{t})$ is given by

$$\tilde{r}^2+[\tilde{h}(\tilde{r},\tilde{t})-\tilde{h}(R_{\rm w},\tilde{t})+R_{\rm w}\cot\alpha]^2=(R_{\rm w}\csc\alpha)^2, \tag{1.1}$$

where the term in the bracket represents the height of the evaporating front above the center of the sphere. Hence the movement of the entire front $\tilde{h}(\tilde{r},\tilde{t})$ can be inferred from the position of the contact line $\tilde{h}(R_{\rm w},\tilde{t})$.

We use the natural scales for the variables:

$$r=\frac{\tilde{r}}{R_{\rm w}},\qquad h(r,t)=\frac{\tilde{h}(\tilde{r},\tilde{t})}{H}, \tag{1.2}$$

where we leave discussion of the time scale to the next section. Substituting (1.2) into (1.1), we obtain

$$R_{\mathrm{w}}^2 r^2 + [Hh(r,t) - Hh(1,\tilde{t}) + R_{\mathrm{w}} \cot\alpha]^2 = (R_{\mathrm{w}} \csc\alpha)^2$$
$$r^2 + [\epsilon^{-1} h(r,t) - \epsilon^{-1} h(1,t) + \cot\alpha]^2 = \csc^2\alpha, \qquad \epsilon = \frac{R_{\mathrm{w}}}{H}. \tag{1.3}$$

We choose the letter ϵ advisedly, since from the Appendix we see that the aspect ratio is much smaller than 1. Therefore to obtain a dominant balance, we must have

$$h(r,t) = h_0(t) + \epsilon h_1(r,t), \qquad h_0(t) = h(1,t), \tag{1.4}$$

and hence to leading order the evaporating front is independent of r. In other words, the movement of the front can be tracked just by tracking the movement of the intersection point with the pore wall.

Some articles specify a receding contact angle for PTFE which is less than $\pi/2$. In that case, the evaporating front is concave, but the leading order is still independent of r due to the scaling.

2 Constant Radius (Adsorption)

We first consider the case where molecules leave the bulk *via* adsorption to the wall and the evaporating front. Since the evaporation rate is so slow (see the Appendix), we ignore convection in the evaporating region, so we have the standard diffusion equation in a cylinder, symmetric in θ:

$$\frac{\partial \tilde{C}}{\partial \tilde{t}} = \tilde{D}\left(\frac{1}{\tilde{r}}\frac{\partial}{\partial \tilde{r}}\left(\tilde{r}\frac{\partial \tilde{C}}{\partial \tilde{r}}\right) + \frac{\partial^2 \tilde{C}}{\partial \tilde{z}^2}\right), \qquad 0 \le \tilde{r} \le R_{\mathrm{w}}, \quad 0 \le \tilde{z} \le \tilde{h}(\tilde{r},\tilde{t}), \tag{2.1}$$

where $\tilde{C}$ is the (volume) concentration in the pore (tube) and $\tilde{D}$ is the diffusion coefficient. In this manuscript we will largely treat $\tilde{D}$ as a scalar constant. All of our work carries over immediately to the case where $\tilde{D}$ depends on $\tilde{C}$; the case where $\tilde{D}$ is a tensor is considered briefly in Sec. 8.

Adsorption occurs when a flux drives molecules to the surface; hence we have

$$-\tilde{D}\frac{\partial \tilde{C}}{\partial \tilde{r}}(R_{\mathrm{w}}, \tilde{z}, \tilde{t}) = \frac{\partial \tilde{\Gamma}_{\mathrm{w}}}{\partial \tilde{t}}, \tag{2.2}$$

where we recall the negative sign in the definition of the flux. Here $\tilde{\Gamma}_{\mathrm{w}}$ is the (surface) concentration adsorbed onto the surface of the tube. (We use the different letter to emphasize the fact that the two concentrations have different units.) Prior to the drying process, the filter is saturated with water and has hence come to some sort of equilibrium already with

some of the concentration already adhered to the surface. Thus we have the following initial conditions:

$$\tilde{C}(\tilde{r},\tilde{z},0)=C_{\rm i}, \qquad \tilde{\Gamma}_{\rm w}(\tilde{z},0)=\tilde{\Gamma}_{\rm w,i}>0. \tag{2.3}$$

Since $\tilde{C}$ is uniform at the initial wet equilibrium, $\tilde{\Gamma}_{\rm w}$ will be as well. Finally, we impose a symmetry condition at the midline of the pore ($\tilde{z}=0$), since the pore is drying from both ends:

$$\frac{\partial \tilde{C}}{\partial \tilde{z}}(\tilde{r},0,\tilde{t})=0. \tag{2.4}$$

We delay discussion of the form of $\tilde{\Gamma}_{\rm w}$ to Section 2.1.

We now make the following simplifying assumptions:

1. We consider concentrations only up to the *critical micelle concentration* (CMC); in other words, the particles do not agglomerate in solution, but rather adhere to the wall as monomers. Note from the Appendix that the CMC is several orders of magnitude larger than the initial concentration, so this seems to be a reasonable assumption.

2. Following the above, in this section we do not consider narrowing of the channel due to the adhesion of the polymers.

To solve these equations, we first introduce scalings into (2.1). We use (1.2) as well as

$$C(r,z,t)=\frac{\tilde{C}(\tilde{r},\tilde{z},\tilde{t})}{C_{\rm i}}, \qquad z=\frac{\tilde{z}}{H}, \qquad t=\frac{\tilde{t}}{t_*}, \tag{2.5a}$$

where we leave the time scale undetermined for now. We use a slightly different factor to normalize $\tilde{\Gamma}_{\rm w}$, for reasons that will become clear below. There are only a certain number of sites on the surface to which the molecules can adsorb. We take these sites as having *area* concentration $\Gamma_{\rm w,T}$, where the subscript "T" stands for "total." Using this quantity to normalize, we obtain

$$\Gamma_{\rm w}(z,t)=\frac{\tilde{\Gamma}_{\rm w}(\tilde{z},\tilde{t})}{\Gamma_{\rm w,T}}. \tag{2.5b}$$

Substituting (1.2) and (2.5) into (2.1), we have

$$\begin{aligned}\frac{C_{\rm i}}{t_*}\frac{\partial C}{\partial t}&=\tilde{D}C_{\rm i}\left[\frac{1}{R^2}\frac{1}{r}\frac{\partial}{\partial r}\left(r\frac{\partial C}{\partial r}\right)+\frac{1}{H^2}\frac{\partial^2 C}{\partial z^2}\right], \qquad 0\le r\le 1, \quad 0\le z\le h(r,t)\\ \frac{\partial C}{\partial t}&=D\left[\epsilon^{-2}\frac{1}{r}\frac{\partial}{\partial r}\left(r\frac{\partial C}{\partial r}\right)+\frac{\partial^2 C}{\partial z^2}\right], \qquad D=\frac{\tilde{D}t_*}{H^2}.\end{aligned} \tag{2.6}$$

Equation (2.6) motivates a perturbation series of the form

$$C(r,z,t;\epsilon)=C_0(r,z,t)+\epsilon^2 C_2(r,z,t)+\cdots. \tag{2.7}$$

Substituting (2.7) into (2.6), we obtain, to leading two orders,

$$D\frac{\partial}{\partial r}\left(r\frac{\partial C_0}{\partial r}\right) = 0, \tag{2.8a}$$

$$D\frac{\partial}{\partial r}\left(r\frac{\partial C_2}{\partial r}\right) = \frac{\partial C_0}{\partial t} - D\frac{\partial^2 C_0}{\partial z^2}. \tag{2.8b}$$

Since r-dependent solutions of (2.8a) have a term of the form $\log r$ that is unphysical at the origin, we surmise that C_0 is a function of z and t only, especially since the leading order of h is also independent of r.

To verify this, we introduce our scalings into (2.2):

$$\begin{aligned}
-\frac{C_\mathrm{i}\tilde{D}}{R_\mathrm{w}}\left(\frac{\partial C_0}{\partial r} + \epsilon^2\frac{\partial C_2}{\partial r}\right)(1,z,t) &= \frac{\Gamma_{\mathrm{w,T}}}{t_*}\frac{\partial \Gamma_\mathrm{w}}{\partial t} \\
-\frac{\tilde{D}t_*}{R_\mathrm{w}^2}\left(\frac{\partial C_0}{\partial r} + \epsilon^2\frac{\partial C_2}{\partial r}\right)(1,z,t) &= \frac{\Gamma_{\mathrm{w,T}}}{R_\mathrm{w}C_\mathrm{i}}\frac{\partial \Gamma_\mathrm{w}}{\partial t} \\
-\frac{D}{\epsilon^2}\left(\frac{\partial C_0}{\partial r} + \epsilon^2\frac{\partial C_2}{\partial r}\right)(1,z,t) &= k_\mathrm{w}\frac{\partial \Gamma_\mathrm{w}}{\partial t}, \qquad k_\mathrm{w} = \frac{\Gamma_{\mathrm{w,T}}}{R_\mathrm{w}C_\mathrm{i}}.
\end{aligned} \tag{2.9}$$

To leading order, we have that

$$\frac{\partial C_0}{\partial r}(1,z,t) = 0,$$

as expected. With no flux at the wall or the centerline, we may conclude that C_0 is a function of z and t only, the specific value of which can be determined by solving (2.8b).

To eliminate the $\partial C_2/\partial r$ term in (2.9), we integrate (2.8b) over r:

$$\begin{aligned}
\int_0^1 \frac{D}{r}\frac{\partial}{\partial r}\left(r\frac{\partial C_2}{\partial r}\right) r\,dr &= \int_0^1 \frac{\partial C_0}{\partial t} - D\frac{\partial^2 C_0}{\partial z^2} r\,dr \\
D\frac{\partial C_2}{\partial r}(1,z,t)\,dr &= \frac{1}{2}\left(\frac{\partial C_0}{\partial t} - D\frac{\partial^2 C_0}{\partial z^2}\right),
\end{aligned} \tag{2.10}$$

where we have used the fact that C_0 is independent of r. Substituting (2.10) into the next order of (2.9) and rearranging, we have

$$\begin{aligned}
-\frac{1}{2}\left(\frac{\partial C_0}{\partial t} - D\frac{\partial^2 C_0}{\partial z^2}\right) &= k_\mathrm{w}\frac{\partial \Gamma_\mathrm{w}}{\partial t} \\
\frac{\partial C_0}{\partial t} &= D\frac{\partial^2 C_0}{\partial z^2} - 2k_\mathrm{w}\frac{\partial \Gamma_\mathrm{w}}{\partial t}, \qquad 0 \le z \le h_0(t).
\end{aligned} \tag{2.11}$$

Note that here we have explicitly indicated that to leading order, the evaporating front is independent of r; the appropriate initial condition is

$$h_0(0) = 1. \tag{2.12a}$$

The remaining conditions are given by using these scalings in (2.3) and (2.4) to obtain

$$C_0(z,0)=1, \qquad \frac{\partial C_0}{\partial z}(0,t)=0, \qquad \Gamma_{\rm w}(z,0)=\Gamma_{\rm i}, \qquad \Gamma_{\rm i}=\frac{\tilde{\Gamma}_{\rm w,i}}{\Gamma_{\rm w,T}}. \tag{2.12b}$$

The system will be closed when we have a condition at the interface $z=h(t)$, which we obtain from concentration of mass. In addition to the concentration *in* the pore, we must also keep track of the concentration *on* the pore, and perhaps one other source of mass. In the same way that the particles can adsorb to the surface, it is also possible that they can adsorb to the evaporation front h. We denote this concentration as $\tilde{\Gamma}_h(\tilde{r},\tilde{t})$; then conservation of mass becomes

$$\frac{d}{d\tilde{t}}\left[2\pi\int_0^{R_{\rm w}}\int_0^{\tilde{h}_0(\tilde{t})}\tilde{C}(\tilde{r},\tilde{z},\tilde{t})\tilde{r}\,d\tilde{z}\,d\tilde{r}+2\pi R_{\rm w}\int_0^{H}\tilde{\Gamma}_{\rm w}(\tilde{z},\tilde{t})\,d\tilde{z}+2\pi\int_0^{R_{\rm w}}\tilde{\Gamma}_h(\tilde{r},\tilde{t})\tilde{r}\,d\tilde{r}\right]=0. \tag{2.13}$$

Introducing our scalings, we have, to leading order,

$$\frac{d}{dt}\left[C_{\rm i}R_{\rm w}^2H\int_0^1\int_0^{h_0(t)}C_0(z,t)r\,dz\,dr+R_{\rm w}H\Gamma_{\rm w,T}\int_0^1\Gamma_{\rm w}(z,t)\,dz+R_{\rm w}^2\Gamma_{h,\rm T}\int_0^1\Gamma_h(t)r\,dr\right]=0,$$

where we note that since C_0 is independent of r, to leading order $\tilde{\Gamma}_h$ will be as well. Thus we define

$$\Gamma_h(t)=\frac{\tilde{\Gamma}_{\rm h}(\tilde{r},\tilde{t})}{\Gamma_{h,\rm T}}, \tag{2.14}$$

in an analogous manner to (2.5b). For notational simplicity, we do not append the subscript 0 to the leading orders of Γ, since we do not need to compute to next order as we do with C.

Continuing to simplify, we obtain

$$\frac{d}{dt}\left[\frac{1}{2}\int_0^{h_0(t)}C_0(z,t)\,dz+\frac{\Gamma_{\rm w,T}}{C_{\rm i}R_{\rm w}}\int_0^1\Gamma_{\rm w}(z,t)\,dz+\frac{\Gamma_{h,\rm T}}{C_{\rm i}H}\frac{\Gamma_h(t)}{2}\right]=0,$$
$$\int_0^{h_0(t)}\frac{\partial C_0}{\partial t}\,dz+\frac{dh_0}{dt}C_0(h_0(t),t)+2k_{\rm w}\int_0^1\frac{\partial\Gamma_{\rm w}}{\partial t}(z,t)\,dz+k_h\frac{d\Gamma_h}{dt}=0, \qquad k_h=\frac{\Gamma_{h,\rm T}}{C_{\rm i}H},$$

where we have used Leibniz's Rule. Substituting (2.11) and (2.12b) into the above yields the following:

$$\int_0^{h_0(t)}D\frac{\partial^2C_0}{\partial z^2}-k_{\rm w}\frac{\partial\Gamma_{\rm w}}{\partial t}\,dz+\frac{dh_0}{dt}C_0(h_0(t),t)+2k_{\rm w}\int_0^1\frac{\partial\Gamma_{\rm w}}{\partial t}(z,t)\,dz=-k_h\frac{d\Gamma_h}{dt}$$
$$D\frac{\partial C_0}{\partial z}(h_0(t),t)+\frac{dh_0}{dt}C_0(h_0(t),t)+2k_{\rm w}\int_{h_0(t)}^1\frac{\partial\Gamma_{\rm w}}{\partial t}(z,t)\,dz=-k_h\frac{d\Gamma_h}{dt}.$$

But the wall concentration doesn't change once the evaporation front has passed by ($h_0(t) < z < 1$), so we obtain

$$D\frac{\partial C_0}{\partial z}(h_0(t),t) + \frac{dh_0}{dt}C_0(h_0(t),t) = -k_h\frac{d\Gamma_h}{dt}. \tag{2.15}$$

Equation (2.15) has a nice physical interpretation: any mass lost through the interface must either contribute to Γ_h or to the wall (which is of concentration $C(h_0(t),t)$ times the differential dh due to the receding of the evaporation front).

However, we note one important fact: here the correction is $O(\epsilon)$ from the next order of h, while in the other sections, the correction is $O(\epsilon^2)$ from the next order of C. Therefore, if we were to calculate the next-order correction, we would have to insert terms in the expansion such as (2.7) at $O(\epsilon)$.

As a final aside, we note that even in situations where the aspect ratio is not small, we can eliminate the r-dependence by examining the cross-sectional average

$$\langle C\rangle(z,t) = 2\int_0^1 C(r,z,t)r\,dr, \tag{2.16}$$

which yields essentially the same equations for $\langle C\rangle$ as those for C_0 in this section.

2.1 Adsorption Constitutive Relations

To further close the system, we need a constitutive equation for the surface concentrations and an equation for the evolution of the evaporation front.

There are several possibilities for the constitutive relation for Γ_{w} and Γ_h. Many of these constitutive models may be found in [8, chap. 5]; first we consider the Langmuir adsorption model

$$\Gamma_\cdot(C) = \frac{K_\cdot C}{1+KC}, \tag{2.17}$$

where K is a normalized equilibrium constant, C is considered to be the value at the interface, and (2.17) could hold for either Γ with appropriate subscript notation (hence the dot where the subscript would be). The Langmuir law is expressed in terms of fractions of adsorption sites, which is why we normalized as in (2.5b). Equation (2.17) can be simplified to

$$\Gamma_\cdot(C) = K_\cdot C \tag{2.18}$$

in the limit of small $K_\cdot$ or small C.

Next we turn our attention to the evaporation rate, which measures the movement of $\tilde{h}$ over time:

$$\frac{\partial\tilde{h}}{\partial\tilde{t}} = -\tilde{E}(\tilde{C}(\tilde{h}(\tilde{t}),\tilde{t}), \qquad \Longrightarrow \qquad \frac{dh_0}{dt} = -E(C(h_0(t),t)), \quad E(C) = \frac{t_*\tilde{E}(\tilde{C})}{H}. \tag{2.19}$$

where E is the evaporation rate. Here we have used the fact that the leading order of $\tilde{h}$ is independent of r to introduce the total derivative. Note that in the simplest case where E

is just a constant, with a particular choice of t_* (namely the evaporation rate), we can force $E = 1$.

More discussion of these issues and more general models for Γ and E are given in Sec. 9.

3 Narrowing Pore Due to Deposition

The porous media can gain as much as 25% in weight after drying, which suggests that the pore may narrow significantly during the drying process. Hence we replace $R_{\rm w}$ with a varying radius $\tilde{R}(\tilde{z},\tilde{t})$. We assume that material precipitates out of solution at the interface rather than adsorbing onto it; hence the boundary condition at the moving wall is given by

$$-\left(\tilde{D}\frac{\partial\tilde{C}}{\partial n}+\frac{\partial\tilde{R}}{\partial\tilde{t}}\tilde{C}\right)(\tilde{R}(\tilde{z},\tilde{t}),\tilde{z},\tilde{t})=\tilde{Q}_{\rm w}(\tilde{C}), \tag{3.1}$$

where $\tilde{Q}_{\rm w}$ is the precipitation flux. A discussion of possible constitutive equations for $\tilde{Q}_{\rm w}$ is given in Section 3.1.

We make several remarks:

1. Comparing the left-hand sides of (2.2) and (3.1), we note that since $\tilde{R}$ is no longer independent of $\tilde{z}$, the derivative in (3.1) is now the normal derivative. Moreover, since the interface is no longer independent of t, there is a convective flux, and the velocity is given by the interface velocity $\partial\tilde{R}/\partial\tilde{t}$.

2. Comparing the right-hand sides of (2.2) and (3.1), we see that $\tilde{Q}_{\rm w}$ plays the role of $\partial\tilde{\Gamma}_{\rm w}/\partial\tilde{t}$, and it will play a similar role in the derivations below. However, we chose different notation since we wanted to emphasize that the physical mechanism is different from adsorption. (Moreover, the correspondence is not exact once constitutive relations are introduced; see Sec. 3.1.) We acknowledge that due to the discussion after (3.13), this mechanism may not be operative in our system, but having a model for other filters should be useful.

3. As $\tilde{Q}_{\rm w}$ is analogous to $\partial\tilde{\Gamma}_{\rm w}/\partial\tilde{t}$, we expect it to be positive. This is consistent with the placement of the minus sign on the left-hand side of (3.1), as both $\partial\tilde{C}/\partial n$ and $\partial\tilde{R}/\partial\tilde{t}$ are negative.

We also note that the radius of the pore will decrease as the solute precipitates onto it; hence we have

$$\frac{\partial\tilde{R}}{\partial\tilde{t}}=-\tilde{\chi}\tilde{Q}_{\rm w}, \tag{3.2}$$

where $\tilde{\chi}$ is a constant.

To solve these equations, we first introduce scalings into (3.1). We use the independent scales from Sec. 2 as well as

$$R(z,t)=\frac{\tilde{R}(\tilde{z},\tilde{t})}{R_{\rm w}}, \tag{3.3}$$

which means that (2.6) now holds on the new domain $0 \le r \le R(z,t)$. (We also note that R should really be expanded in powers of ϵ as in (2.7). However, since we are solving only to leading order, we ignore that detail for now, as we did for Γ in the previous section.)

To verify that C_0 is still independent of r, we simplify (3.1). First we note that the appropriate direction for the normal derivative will be given by

$$\left(1, -\frac{\partial \tilde{R}}{\partial \tilde{z}}\right) = \left(1, -\frac{R_\mathrm{w}}{H}\frac{\partial R}{\partial z}\right) = \left(1, -\epsilon\frac{\partial R}{\partial z}\right), \tag{3.4}$$

which is also equal to the *normal* vector, up to $O(\epsilon^2)$. Using that result and our scalings in (3.1), we obtain, to leading order,

$$\begin{aligned}
-\left[C_\mathrm{i}\tilde{D}\left(\frac{1}{R_\mathrm{w}}\frac{\partial C}{\partial r}, \frac{1}{H}\frac{\partial C}{\partial z}\right)\cdot\left(1, -\epsilon\frac{\partial R}{\partial z}\right) + \frac{R_\mathrm{w}}{t_*}\frac{\partial R}{\partial t}C_\mathrm{i}C\right](R(z,t),z,t) &= \tilde{Q}_\mathrm{w}(\tilde{C}) \\
-\left[\frac{\tilde{D}t_*}{R_\mathrm{w}^2}\left(\frac{\partial C}{\partial r}, \epsilon\frac{\partial C}{\partial z}\right)\cdot\left(1, -\epsilon\frac{\partial R}{\partial z}\right) + \frac{\partial R}{\partial t}C\right](R(z,t),z,t) &= \frac{t_*}{C_\mathrm{i}R_\mathrm{w}}\tilde{Q}_\mathrm{w}(\tilde{C}) \\
-\left[\frac{D}{\epsilon^2}\left(\frac{\partial C}{\partial r}, \epsilon\frac{\partial C}{\partial z}\right)\cdot\left(1, -\epsilon\frac{\partial R}{\partial z}\right) + \frac{\partial R}{\partial t}C\right](R(z,t),z,t) &= Q_\mathrm{w}(C), \qquad \text{(3.5a)} \\
Q_\mathrm{w}(C) &= \frac{t_*}{C_\mathrm{i}R_\mathrm{w}}\tilde{Q}_\mathrm{w}(\tilde{C}). \qquad \text{(3.5b)}
\end{aligned}$$

The leading order is $O(\epsilon^{-2})$, and the balance (as expected) is that $\partial C_0/\partial r = 0$ at the deposition interface, so we may conclude that C_0 is again a function of z and t only.

Using this fact, we have that the next order is given by

$$-\left[\frac{D}{\epsilon^2}\left(\epsilon^2\frac{\partial C_2}{\partial r}, \epsilon\frac{\partial C_0}{\partial z}\right)\cdot\left(1, -\epsilon\frac{\partial R}{\partial z}\right) + \frac{\partial R}{\partial t}C_0\right](R(z,t),z,t) = Q_\mathrm{w}(C_0), \tag{3.6}$$

and hence the $O(\epsilon^2)$ correction to the normal vector does not contribute at this order either. Multiplying the $O(1)$ terms by $R(z)$ and rearranging, we obtain the following:

$$-DR(z,t)\frac{\partial C_2}{\partial r}(R(z,t),z,t) = -D\frac{\partial C_0}{\partial z}R(z,t)\frac{\partial R}{\partial z} + R(z,t)\frac{\partial R}{\partial t}C_0 + R(z,t)Q_\mathrm{w}(C_0), \tag{3.7}$$

To eliminate the $\partial C_2/\partial r$ term in (3.7), we integrate (2.8b) over r:

$$\begin{aligned}
\int_0^{R(z,t)} \frac{D}{r}\frac{\partial}{\partial r}\left(r\frac{\partial C_2}{\partial r}\right) r\,dr &= \int_0^{R(z,t)} \frac{\partial C_0}{\partial t} - D\frac{\partial^2 C_0}{\partial z^2} r\,dr \\
DR(z,t)\frac{\partial C_2}{\partial r}(R(z,t),z,t)\,dr &= \left(\frac{\partial C_0}{\partial t} - D\frac{\partial^2 C_0}{\partial z^2}\right)\frac{[R(z,t)]^2}{2}, \qquad \text{(3.8)}
\end{aligned}$$

where we have used the fact that C_0 is independent of r. Substituting (3.8) into (3.7) and rearranging, we have

$$-D\frac{1}{2}\frac{\partial C_0}{\partial z}\frac{\partial [R(z,t)]^2}{\partial z}+\frac{1}{2}C_0\frac{\partial [R(z,t)]^2}{\partial t}+R(z,t)Q_{\rm w}(C_0)=-\left(\frac{\partial C_0}{\partial t}-D\frac{\partial^2 C_0}{\partial z^2}\right)\frac{[R(z,t)]^2}{2}$$

$$\frac{\partial (C_0[R(z,t)]^2)}{\partial t}=D\frac{\partial}{\partial z}\left([R(z,t)]^2\frac{\partial C_0}{\partial z}\right)-2R(z,t)Q_{\rm w}(C_0). \tag{3.9}$$

We make two remarks:

1. If there is no deposition, $R(z,t)=1$ and (3.9) reduces to a very similar form to (2.11), again with $Q_{\rm w}$ playing the role of $\partial\Gamma_{\rm w}/\partial t$.
2. Note that (3.9) can also probably be derived using a mass balance in an infinitesimal disc.

This equation would then be coupled to the scaled version of the deposition equation (3.2):

$$\begin{aligned}\frac{R_{\rm w}}{t_*}\frac{\partial R}{\partial t}&=-\tilde{\chi}\tilde{Q}_{\rm w}(\tilde{C})\\ \frac{\partial R}{\partial t}&=-\tilde{\chi}C_{\rm i}\frac{t_*}{C_{\rm i}R_{\rm w}}\tilde{Q}_{\rm w}=-\chi Q_{\rm w}(C_0),\qquad \chi=\tilde{\chi}C_{\rm i}.\end{aligned} \tag{3.10}$$

This PDE requires an initial condition. Again, we expect the system to be in a "wet equilibrium" at $t=0$. Since this equilibrium will have a uniform concentration, we expect that $R(z,0)$ will be uniform in z as well:

$$R(z,0)=R_{\rm i}\le 1, \tag{3.11}$$

where we take into account that if the wet equilibrium concentration (in the absence of deposition) is greater than the saturation concentration $C_{\rm sat}$, then deposition will occur and $R_{\rm i}<1$. (In that case, $C_{\rm i}=C_{\rm sat}$, since the equilibrium will then be determined by the absence of deposition.)

The system is closed once we derive an equation analogous to (2.15). In this case, conservation of mass becomes

$$\frac{d}{d\tilde{t}}\left[2\pi\int_0^{\tilde{h}_0(\tilde{t})}\int_0^{\tilde{R}(\tilde{z},\tilde{t})}\tilde{C}(\tilde{r},\tilde{z},\tilde{t})\tilde{r}\,d\tilde{r}\,d\tilde{z}+2\pi\int_0^H\int_0^{\tilde{t}}\tilde{Q}_{\rm w}(\tilde{C})\tilde{R}(\tilde{z},\tilde{t}')\,d\tilde{t}'\,d\tilde{z}\right]=0.$$

Here the first term tracks the mass in the liquid, and the second term tracks the mass that has deposited over time. We make the following remarks:

1. This isn't technically correct if $R_{\rm i}<1$, as it doesn't track the mass that has deposited before $t=0$. But since that mass is never removed (since C is always increasing), it won't contribute to the derivative.

2. We are ignoring any adsorption at the evaporation front, but this may easily be added in a manner analogous to (2.13).

Introducing our scalings, we have, to leading order,

$$H\frac{d}{dt}\left[C_{\mathrm{i}}R_{\mathrm{w}}^2\int_0^{h_0(t)}\int_0^{R(z,t)}C_0(z,t)r\,dr\,dz + t_*\int_0^1\int_0^t\frac{C_{\mathrm{i}}R_{\mathrm{w}}}{t_*}Q_{\mathrm{w}}(C_0)R_{\mathrm{w}}R(z,t)\,dt'\,dz\right] = 0$$

$$\frac{d}{dt}\left[\int_0^{h_0(t)}C_0(z,t)\frac{[R(z,t)]^2}{2}\,dz + \int_0^t\int_0^1 Q_{\mathrm{w}}(C_0)R(z,t')\,dz\,dt'\right] = 0$$

$$\frac{1}{2}\int_0^{h_0(t)}\frac{\partial(C_0[R(z,t)]^2)}{\partial t}\,dz + \frac{1}{2}\frac{dh_0}{dt}C_0(h_0(t))[R(h_0(t),t)]^2 + \int_0^1 Q_{\mathrm{w}}(C_0)R(z,t)\,dz = 0,$$

where we have used Leibniz's Rule. Continuing to simplify using (3.9), we obtain

$$\int_0^{h_0(t)}D\frac{\partial}{\partial z}\left([R(z,t)]^2\frac{\partial C_0}{\partial z}\right) - 2R(z,t)Q_{\mathrm{w}}(C_0)\,dz$$
$$+\frac{dh_0}{dt}C_0(h_0(t))[R(h_0(t),t)]^2 + 2\int_0^{h_0(t)}Q_{\mathrm{w}}(C_0)R(z,t)\,dz = 0,$$

where we have used the fact that there is no deposition above the evaporation front. Continuing to simplify, we have the following:

$$D[R(h_0(t),t)]^2\frac{\partial C_0}{\partial z}(h_0(t),t) + \frac{dh_0}{dt}C_0(h_0(t))[R(h_0(t),t)]^2 = 0$$
$$D\frac{\partial C_0}{\partial z}(h_0(t),t) + \frac{dh_0}{dt}C_0(h_0(t)) = 0, \tag{3.12}$$

which is exactly (2.15) when the front adsorption Γ_h is neglected.

3.1 Deposition Constitutive Relations

To close the system, we need a constitutive relation for how Q_{w} depends on C. If C is greater than the saturation concentration C_{sat}, the particles precipitate out and stick to the surface. One function that models this is

$$\tilde{Q}_{\mathrm{w}} = \tilde{\lambda}(\tilde{C}-\tilde{C}_{\mathrm{sat}})H(\tilde{C}-\tilde{C}_{\mathrm{sat}}) \equiv \tilde{\lambda}(\tilde{C}-\tilde{C}_{\mathrm{sat}})^+$$
$$Q_{\mathrm{w}} = \frac{t_*}{C_{\mathrm{i}}R_{\mathrm{w}}}\tilde{\lambda}C_i(C-C_{\mathrm{sat}})^+$$
$$= \lambda(C-C_{\mathrm{sat}})^+, \qquad \lambda = \frac{t_*\tilde{\lambda}}{R_{\mathrm{w}}}, \tag{3.13}$$

where we have used (3.5b). Here $\lambda > 0$ is a constant.

Theoretically, there may be an objection to this form because it is irreversible. In other words, if C somehow declined below $C_{\rm sat}$, then we would expect the particles to detach from the wall and return to solution, rendering $Q_{\rm w} < 0$, which is forbidden by the form of (3.13). Physically this should not happen, because C is growing as a function of time due to the evaporation front reducing the volume. Indeed this is the behavior seen experimentally.

Moreover, the CMC concentration $C_{\rm CMC}$ is less than $C_{\rm sat}$, so micelles would form before deposition happens. And recall that we are doing all our computations in the regime where $C < C_{\rm CMC}$, as we do not include the complications associated with micelle formation.

With the constitutive relation in (3.13), it is possible for $R(z, t_{\rm c}) = 0$ for some time $t_{\rm c}$ before the liquid evaporates completely. At that point, we consider the pore to be clogged (hence the subscript "c"), and our computations end at that point.

Note that with the choice of constitutive relations, the difference between the adsorption and deposition cases becomes clear. In particular, using the linear relation (3.13) will introduce a term proportional to C in (3.9). However, using the analogous relation (2.18) in (2.11) will introduce a term proportional to $\partial C_0/\partial t$.

3.2 Numerical Calculations

We solve the deposition model by using the method of lines in `Mathematica 12.1`. Here we take the evaporation rate E to be a constant equal to 1, so we have

$$\frac{dh_0}{dt} = -1. \tag{3.14}$$

Moreover, in this section for each figure all of the dimensionless parameters are considered to be 1, except when stated otherwise.

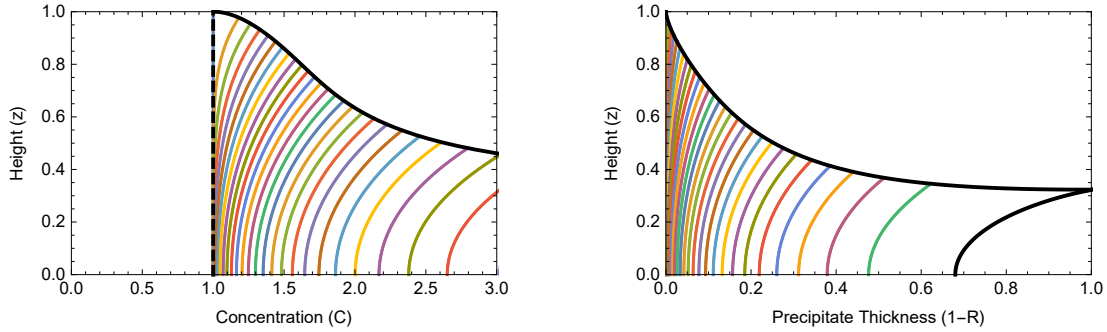

Figure 3.1: Solutions *vs.* height, all parameters equal to 1. Upper black curve is evaporation front. Colored curves denote solutions at uniformly spaced times between 0 and $t_{\rm c}$. (Spacing is the same for both graphs, though fewer are shown at left.) Left: Concentration field; dotted black line indicates the value of $C_{\rm sat} = 1$. Right: Deposited thickness; lower black curve represents final distribution at $t_{\rm c}$.

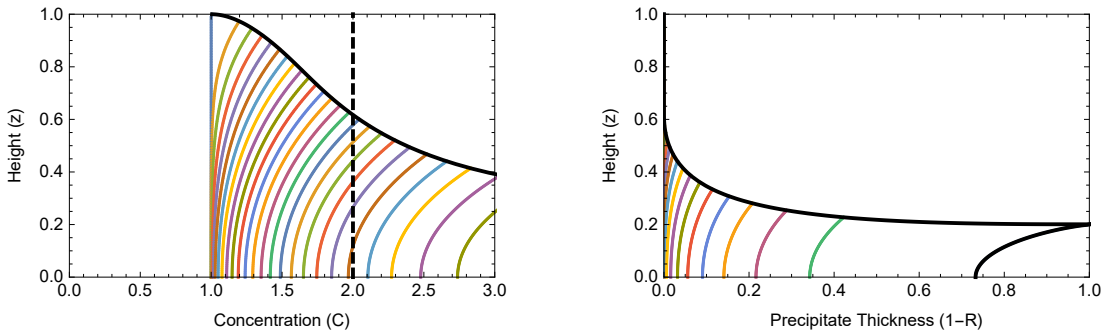

Figure 3.2: Solutions *vs.* height as in Fig. 3.1, except $C_{\rm sat} = 2$ (the rest of the parameters are equal to 1.)

Figure 3.1 shows a representative solution of model with all parameters set equal to 1. Since the saturation concentration is the initial concentration, deposition begins immediately. As the concentration increases with height, greater deposition occurs near the evaporation front. Note that the filter clogs totally at some finite time.

In Fig. 3.2, the saturation concentration has been taken equal to 2. Thus some evaporation occurs before deposition occurs, as shown at right. Consequently, $t_{\rm c}$ is larger, corresponding to a higher deposition thickness at $z = 0$.

Figure 3.3 shows the effect of D on the solution. In particular, when D is small, C becomes quite large near the evaporating front, with a steep gradient to the bulk. Hence the bulk of the deposition happens at the evaporation front, with very little beneath, as shown at top right. In contrast, if D is large, C is nearly uniform in height. This results in nearly uniform deposition, as shown at bottom right.

Figure 3.4 shows the effect of the reaction rate χ on the solution. In particular, increasing χ increases the rate of narrowing for a given precipitation flux. Hence the channel occludes much more rapidly, as shown in the bottom graph.

Figures 3.5 and 3.6 show the effect of the deposition coefficient λ on the solution. In particular, increasing λ increases the precipitation flux given a particular concentration profile. Hence a larger value of λ will lead to faster pore occlusion, as shown in the bottom graph of Fig. 3.5 and the graphs in Fig. 3.6.

The relationship between clogging height and λ is shown directly in Fig. 3.7. As discussed, increasing λ increases the clogging process, which moves the final clogging height upward from $z = 0$, until it asymptotes to $z = 1$ for very large values of λ.

4 Large-D Asymptotics

Looking at the numerics for large diffusion, we conclude that the concentration is approximately a function of time alone (see Fig. 3.3). This means there is an underlying asymptotic structure to be exploited. We expect $D \gg 1$, and so we rewrite our variable in powers of

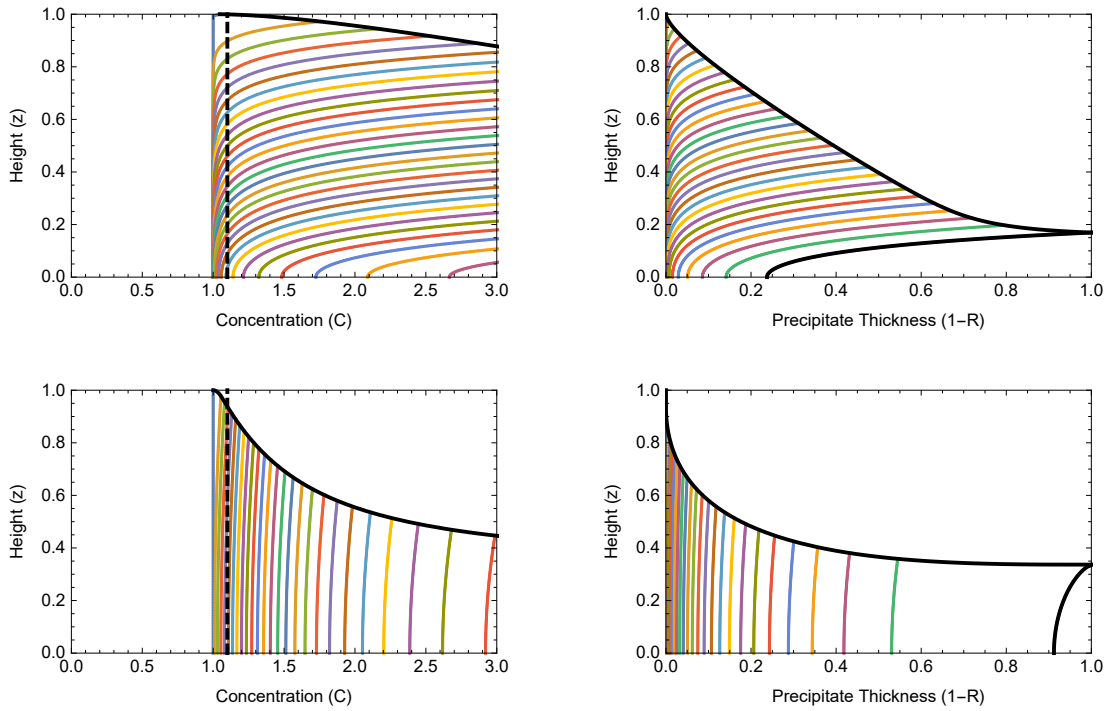

Figure 3.3: Comparison of effect of D on solution profiles, which are as in Fig. 3.1, except $C_{\rm sat} = 1.1$. Top: $D = 0.1$. Bottom: $D = 10$. The rest of the parameters are equal to 1.

D^{-1}. As we have already used a subscript for C in (2.7), we use a slightly different notation:

$$C_0(x,t;D) \sim \mathcal{C}_0(x,t) + D^{-1}\mathcal{C}_1(x,t) + \cdots . \tag{4.1}$$

Note that in order for us to neglect C_2 in favor of the expression (4.1), $\epsilon^2 = o(D^{-1})$.

4.1 Adsorption

We begin by considering the adsorption case. Substituting (4.1) into (2.11), (2.15), and the no-flux condition in (2.12b), we have, to leading two orders,

$$\frac{\partial^2 \mathcal{C}_0}{\partial z^2} = 0, \quad \frac{\partial \mathcal{C}_0}{\partial z}(h_0(t),t) = 0, \quad \frac{\partial \mathcal{C}_0}{\partial z}(0,t) = 0. \tag{4.2}$$

$$\frac{\partial \mathcal{C}_0}{\partial t} + 2k_{\rm w}\frac{\partial \Gamma_{\rm w}}{\partial t}(\mathcal{C}_0) = \frac{\partial^2 \mathcal{C}_1}{\partial z^2}, \tag{4.3a}$$

$$\frac{\partial \mathcal{C}_1}{\partial z}(h_0(t),t) + \frac{dh_0}{dt}\mathcal{C}_0(h_0(t),t) = -k_h\frac{d\Gamma_h}{dt}(\mathcal{C}_0), \quad \frac{\partial \mathcal{C}_1}{\partial z}(0,t) = 0 \tag{4.3b}$$

Thus, solving (4.2), we obtain that $\mathcal{C}_0$ is a function of time alone, as expected.

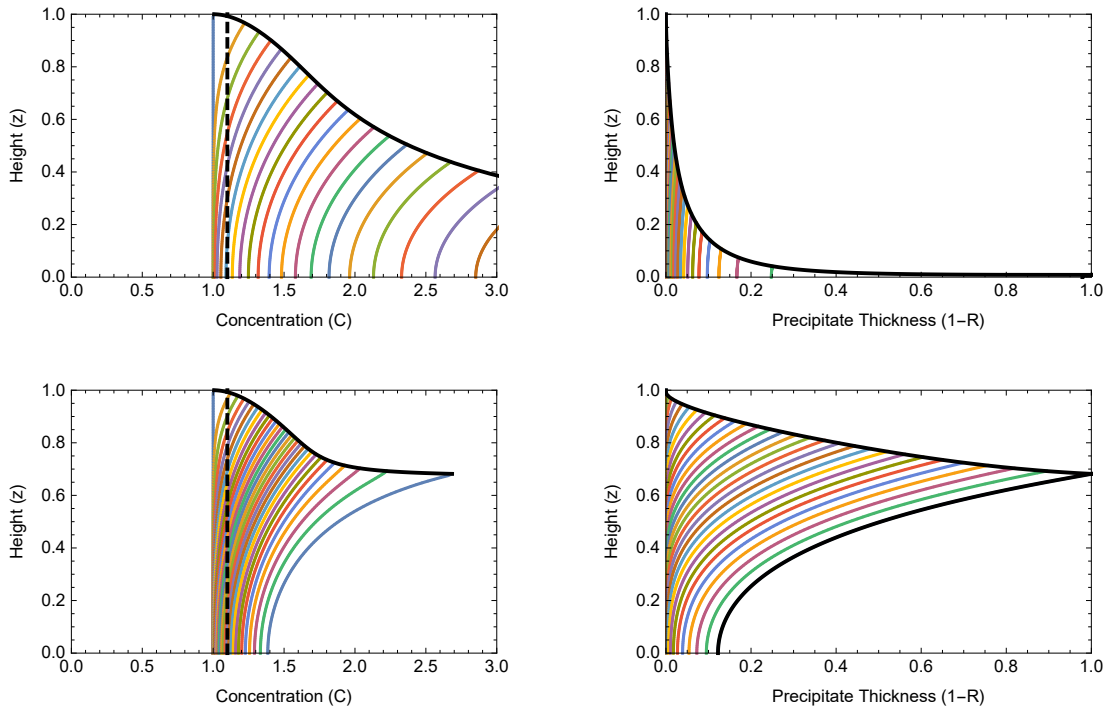

Figure 3.4: Comparison of effect of reaction rate χ on solution profiles, which are as in Fig. 3.3, except $D = 1$. Top: slow reaction rate ($\chi = 0.1$). Bottom: fast reaction rate ($\chi = 10$).

This fact implies that the left-hand side of (4.3a) is independent of z; hence we may integrate that equation from $z = 0$ to $h_0(t)$ to obtain

$$h_0\left[\frac{d\mathcal{C}_0}{dt} + 2k_{\rm w}\frac{d\Gamma_{\rm w}}{dt}(\mathcal{C}_0)\right] = \left.\frac{\partial \mathcal{C}_1}{\partial z}\right|_{z=0}^{z=h} = -k_h\frac{d\Gamma_h}{dt}(\mathcal{C}_0) - \frac{dh_0}{dt}\mathcal{C}_0(t)$$
$$\frac{d(h_0\mathcal{C}_0)}{dt} = -k_h\frac{d\Gamma_h}{dt}(\mathcal{C}_0) - 2h_0k_{\rm w}\frac{d\Gamma_{\rm w}}{dt}(\mathcal{C}_0), \tag{4.4}$$

where in the first line we have used (4.3b) and the fact that $\mathcal{C}_0$ is independent of time. Note that (4.4) has a nice physical interpretation: the change in the total concentration must be lost either to the evaporating surface or the walls.

Since we are considering the case of surface adsorption where the walls do not narrow, we use the constitutive relations in Sec. 2.1. In particular, using the linear functional forms

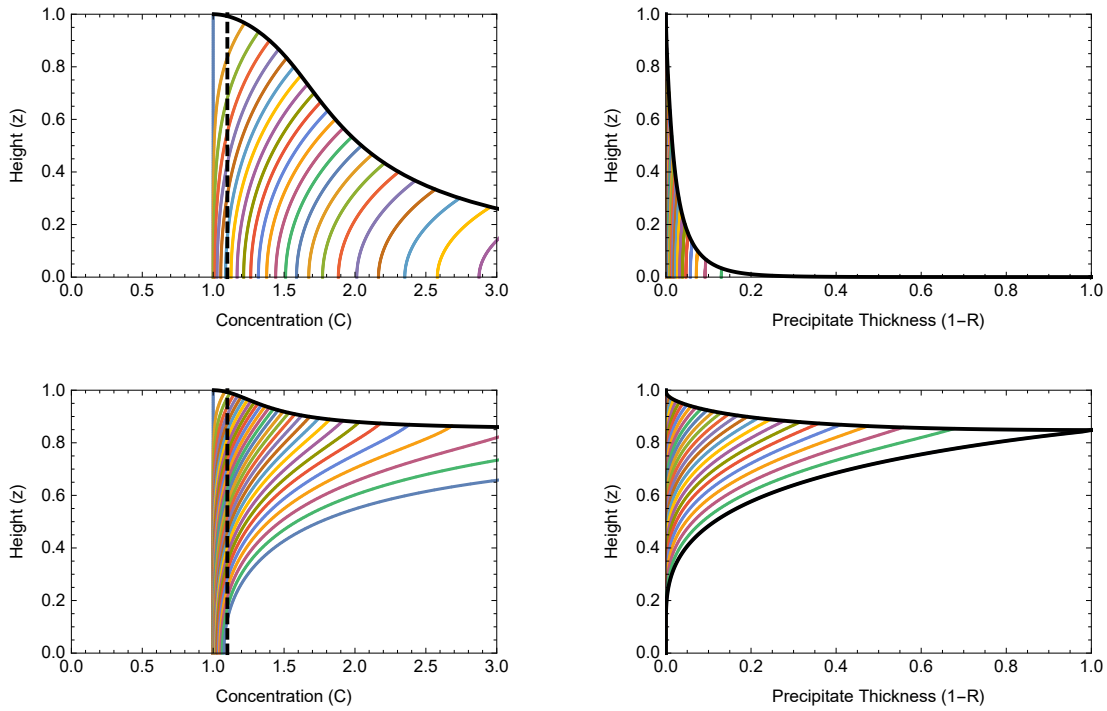

Figure 3.5: Comparison of effect of deposition coefficient λ on solution profiles, which are as in Fig. 3.3, except $D = 1$. Top: small deposition coefficient ($\lambda = 0.1$). Bottom: large deposition coefficient ($\lambda = 10$).

in (2.18) for the Γ, (4.4) becomes

$$
\begin{aligned}
h_0\frac{d\mathcal{C}_0}{dt} + \frac{dh_0}{dt}\mathcal{C}_0 &= -k_hK_h\frac{d\mathcal{C}_0}{dt} - 2h_0k_{\mathrm{w}}K_{\mathrm{w}}\frac{d\mathcal{C}_0}{dt}\\
[h_0(1+2k_{\mathrm{w}}K_{\mathrm{w}}) + k_hK_h]\frac{d\mathcal{C}_0}{dt} + \frac{dh_0}{dt}\mathcal{C}_0 &= 0\\
\frac{d}{dt}\left(\left[\frac{h_0}{\beta} + k_hK_h\right]^{\beta}\mathcal{C}_0\right) &= 0, \quad \beta = \frac{1}{1+2k_{\mathrm{w}}K_{\mathrm{w}}},\\
\mathcal{C}_0(t) &= \left(\frac{1+\beta k_hK_h}{h_0+\beta k_hK_h}\right)^{\beta},
\end{aligned}
\tag{4.5}
$$

where we have used (2.12a) and the leading order of the initial condition in (2.12b). Since h_0 is decreasing as time increases, the concentration indeed increases as t increases.

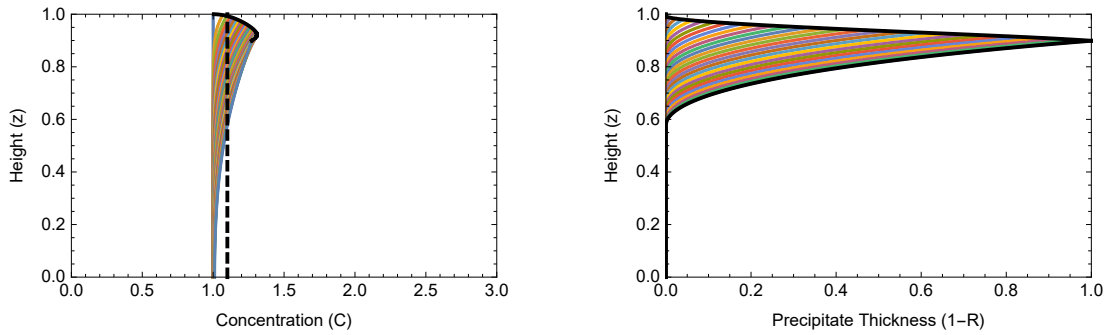

Figure 3.6: A case of fast clogging due to high reaction rate. Solution profiles are as in Fig. 3.4, except $\lambda = 100$.

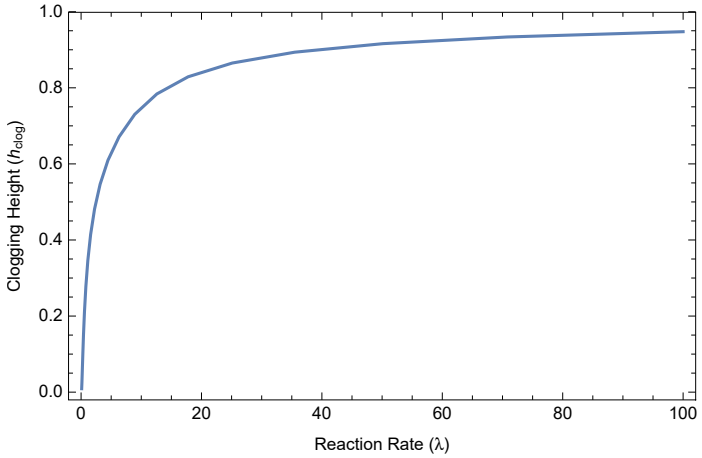

Figure 3.7: Clogging height as a function of the reaction rate. $C_{\text{sat}} = 1.1$, and all the rest of the parameters are considered to be 1.

4.2 Deposition

Now we consider the case of deposition on the walls. In this case, (2.11) is replaced by (3.9); substituting in (4.1) yields, to leading two orders,

$$\frac{\partial}{\partial z}\left([R(z,t)]^2\frac{\partial \mathcal{C}_0}{\partial z}\right) = 0 \tag{4.6a}$$

$$\frac{\partial(\mathcal{C}_0[R(z,t)]^2)}{\partial t} + 2R(z,t)Q_{\text{w}}(\mathcal{C}_0) = \frac{\partial}{\partial z}\left([R(z,t)]^2\frac{\partial \mathcal{C}_1}{\partial z}\right). \tag{4.6b}$$

Solving (4.6a) subject to the boundary conditions in (4.2), we again find that $\mathcal{C}_0$ is a function of time alone. Using that fact in (3.10), we conclude that

$$R(z,t) = R_0(t) + O(D^{-1}). \tag{4.7}$$

Then integrating (4.6b) in z as before, but using the appropriate expansion of (3.12) instead of (4.3b), we obtain the following:

$$h_0\left(\frac{1}{2}\frac{\partial(R_0^2\mathcal{C}_0)}{\partial t}+R_0Q_{\rm w}(\mathcal{C}_0)\right)=\frac{R_0^2}{2}\frac{\partial\mathcal{C}_1}{\partial z}\bigg|_{z=0}^{z=h}=-\frac{R_0^2}{2}\frac{dh_0}{dt}\mathcal{C}_0$$

$$\frac{1}{2}\frac{d(h_0R_0^2\mathcal{C}_0)}{dt}=-h_0R_0Q_{\rm w}(\mathcal{C}_0). \tag{4.8}$$

Since we are considering the case of deposition where the walls do narrow, we use the constitutive relations in Sec. 3.1. For simplicity, we use the constitutive relation in (3.13), as well as (3.14). Then in Fig. 4.1 we plot the spatial deposition profile for R_0 when $C_{\rm sat}=1.1$, $\chi=0.1$. We see that the pore has shrunken by around 20% in the case of moderate take-up ($\lambda=1$), and it clogs up very fast when $\lambda=10$.

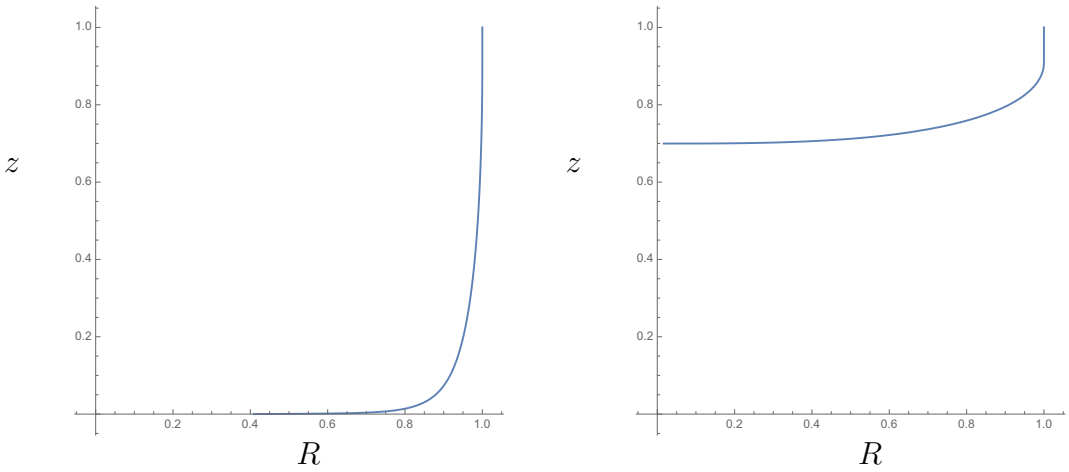

Figure 4.1: Plot of the final layer thickness along the pore (deposition) with $\lambda=1$ (left) and $\lambda=10$ (right).

5 Large-λ Asymptotic Limit

As shown in Fig. 3.6, numerical solutions of the deposition process (3.13) for large precipitation rate λ suggest that clogging happens quickly once the saturation concentration has been reached; this is also indicated in the figure at right of Fig. 4.1. Therefore, we consider the asymptotic limit of large λ.

From (3.13), we see that with $\lambda\gg1$, the consequent large saturation rate will force clogging to occur very quickly after $C>C_{\rm sat}$. From the figures in Sec. 3.2, the concentration

is largest at the evaporation front. Therefore, let t_{sat}, the time at which the solution is first saturated, be defined by

$$C(h_0(t_{\text{sat}}), t_{\text{sat}}) = C_{\text{sat}}. \tag{5.1}$$

Since clogging occurs for small time near the evaporation front, we introduce the following scalings:

$$\hat{t} = (t - t_{\text{sat}})\lambda^{1/2}, \qquad \hat{z} = [h_0(t_{\text{sat}}) - z]\lambda^{1/2}, \qquad \hat{C}(\hat{z}, \hat{t}) = [C_0(z,t) - C_{\text{sat}}]\lambda^{1/2} \tag{5.2a}$$

$$\hat{h}(\hat{t}) = [h_0(t_{\text{sat}}) - h_0(t)]\lambda^{1/2}. \tag{5.2b}$$

Note that we have chosen the $\hat{z}$ scaling so that $\hat{z} \geq 0$. These scalings define a small saturated layer near the evaporating front.

Substituting (5.2) into (3.13) and (3.10), we obtain

$$Q_{\text{w}} = \lambda(\lambda^{-1/2}\hat{C})^{+} \qquad \Longrightarrow \qquad \lambda^{1/2}\frac{\partial R}{\partial \hat{t}} = -\chi\lambda^{1/2}\hat{C}^{+}. \tag{5.3}$$

Substituting (5.2) and (5.3) into (3.9), we have, to leading order,

$$\begin{aligned}
\lambda^{1/2}\frac{\partial(R^2 C_{\text{sat}})}{\partial \hat{t}} &= D\lambda^{1/2}\frac{\partial}{\partial \hat{z}}\left(R^2\frac{\partial \hat{C}}{\partial \hat{z}}\right) - 2R\lambda^{1/2}\hat{C}^{+} \\
2RC_{\text{sat}}\frac{\partial R}{\partial \hat{t}} &= D\frac{\partial}{\partial \hat{z}}\left(R^2\frac{\partial \hat{C}}{\partial \hat{z}}\right) - 2R\hat{C}^{+} \\
D\frac{\partial}{\partial \hat{z}}\left(R^2\frac{\partial \hat{C}}{\partial \hat{z}}\right) &= 2(1 - \chi C_{\text{sat}})R\hat{C}^{+}.
\end{aligned} \tag{5.4}$$

Substituting (5.2) into (3.12) and expanding to leading order, we obtain one boundary condition on (5.4):

$$-D\frac{\partial \hat{C}}{\partial \hat{z}}(\hat{h}(\hat{t}), \hat{t}) - \frac{d\hat{h}}{d\hat{t}}C_{\text{sat}} = 0, \tag{5.5a}$$

The second condition is given by matching to the outer solution $C = C_{\text{sat}}$:

$$\hat{C} \to 0 \qquad \text{as} \qquad \hat{z} \to \infty. \tag{5.5b}$$

In Fig. 5.1 we plot numerical solutions of (5.4) and (5.5) using (3.14). In particular, we show the free space in the pore R over the pore length for different times.

To obtain some additional analytical insight into our problem, we derive the small-$\hat{t}$ profile for $\hat{C}$. Initially $R \approx 1$ and $\hat{h} \approx 0$, so (5.4) and (5.5a) become

$$\frac{\partial^2 \hat{C}}{\partial \hat{z}^2} \approx \frac{2(1 - \chi C_{\text{sat}})}{D}\hat{C}, \qquad D\frac{\partial \hat{C}}{\partial \hat{z}}(0, \hat{t}) \approx -\frac{d\hat{h}}{d\hat{t}}C_{\text{sat}} \tag{5.6}$$

Since χ is small, we take $\chi C_{\text{sat}} < 1$ in (5.6), in which case our solution is found to be

$$\hat{C} = \frac{C_{\text{sat}}}{\sqrt{2(1 - \chi C_{\text{sat}})D}}\frac{d\hat{h}}{d\hat{t}}\exp\left(-\sqrt{\frac{2(1 - \chi C_{\text{sat}})}{D}}\hat{z}\right). \tag{5.7}$$

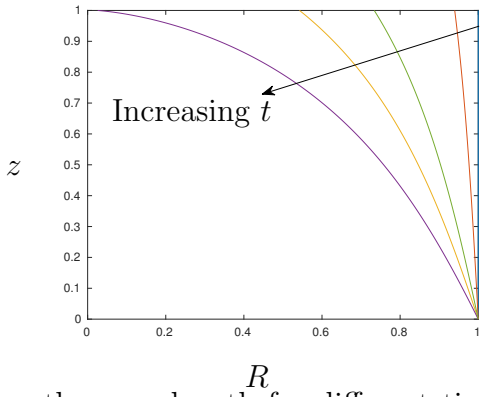

Figure 5.1: Plot of R along the pore length for different times: $t = 0$, $t = 0.01$, $t = 0.05$, $t = 0.1$, $t = 1$. Parameters used: $\chi = 1, C_{\text{sat}} = 1.1, D = 1$.

6 Long-Wave Model for the Exterior Problem

The nature of the ePTFE membrane material is generally a random matrix of polymer fibers rather than being a porous material with pores channeling through a solid substrate. This motivates re-examining the analysis from the previous sections in a complementary form – rather than for transport inside a cylindrical pore (clogging of a pipe), consider the exterior problem outside a cylindrical polymer fiber. Over considerable lengths of the fibers, there is a moderate empty space (on the order of 5–10 diameters) between them and the rest of the matrix (accumulation on nodes, or junctions of fibers, can be considered as an exterior problem on an idealized spherical geometry). The lengths of the fibers are much longer, so a long-wave analysis can still be applied with $\epsilon = R_{\text{w}}/H \ll 1$, where R_{w} is now considered to be the initial fiber radius, rather than the initial pore radius.

We follow the derivation in Sec. 3, except that we consider the domain $R(z,t) \leq r \leq F$, where $R(z,t)$ is the fiber radius (including any accrued precipitation) and F is a far-field radius with $F = O(10)$. At $r = F$, we either impose a no-flux condition

$$\frac{\partial C}{\partial r}(F,z,t) = 0, \tag{6.1a}$$

or a Robin-type boundary condition describing the far-field concentration approaching a constant level, call it "C_∞" as in

$$D\frac{\partial C}{\partial r}(F,z,t) = \epsilon^2 k[C(F,z,t) - C_\infty], \tag{6.1b}$$

where k is an $O(1)$ constant. Note the presence of the ϵ^2 on the right-hand side of (6.1b) is a consequence of the scaling. Nevertheless, its presence implies that to leading order, there is no flux through F no matter which of (6.1) we choose. Hence (as before) at leading order we find that the solution is independent of r due to the leading order no-flux boundary condition at the surface of the fiber (assuming slow attachment rate).

Then integrating (2.8b) from $R \leq r \leq F$, we obtain

$$\frac{F^2 - R^2(z,t)}{2}\frac{\partial C_0}{\partial t} = \frac{F^2 - R^2(z,t)}{2}D\frac{\partial^2 C_0}{\partial z^2} + FD\frac{\partial C_2}{\partial r}(F,z,t) - RD\frac{\partial C_2}{\partial r}(R(z,t),z,t), \quad (6.2)$$

which is analogous to (3.8). When introducing the deposition flux, we note that since the fiber is now the *inner* radius, rather than the *outer* one, the normal is oriented in the opposite direction to that in (3.1). The mathematical upshot is that we may replace Q_{w} by $-Q_{\mathrm{w}}$ in the work in Sec. 3.

In particular, changing the sign of Q_{w} in (3.7) and substituting the result into (6.2), we have the following:

$$\frac{\partial}{\partial t}\left(\frac{F^2 - R^2}{2}C_0\right) = \frac{\partial}{\partial z}\left(\frac{F^2 - R^2}{2}D\frac{\partial C_0}{\partial z}\right) + FD\frac{\partial C_2}{\partial r}(F,z,t) - RQ_{\mathrm{w}}. \quad (6.3)$$

This is not the final form, as we must utilize the C_2 boundary term at $r = F$. Using (6.1a) will eliminate the term to yield

$$\frac{\partial}{\partial t}\left(\frac{F^2 - R^2}{2}C_0\right) = \frac{\partial}{\partial z}\left(\frac{F^2 - R^2}{2}D\frac{\partial C_0}{\partial z}\right) - RQ_{\mathrm{w}}, \quad (6.4a)$$

which is very similar to (3.9). Using (6.1b) would yield a governing equation of the form

$$\frac{\partial}{\partial t}\left(\frac{F^2 - R^2}{2}C_0\right) = \frac{\partial}{\partial z}\left(\frac{F^2 - R^2}{2}D\frac{\partial C_0}{\partial z}\right) + kF(C_0 - C_\infty) - RQ_{\mathrm{w}}. \quad (6.4b)$$

The significance of the extra C_∞ term (which could be generalized to depend on time) is that of a mean field, allowing for a global coupling of fibers, which could hopefully lead to constructing a spatially homogenized model for the evolution of a spatially dependent $\langle R(z,t)\rangle$ (corresponding to variations in imposed initial concentrations and/or variations in fiber properties).

The governing equation for C_0 would then be coupled to (3.10) with the sign of Q_{w} again reversed:

$$\frac{\partial R}{\partial t} = \chi Q_{\mathrm{w}}(C_0), \quad (6.5)$$

where we note that the deposition flux will now cause R to grow.

7 Ideas for Multiple Fiber Models in the $D \gg 1$ Limit

Let's go back to a simpler version of the previous section and look at the $D \gg 1$ limit. A fiber with radius $R(z,t)$ is in the middle of a cylinder with radius F which is assumed to contain the fluid. Therefore, we consider the dimensionless equation (2.6), but instead of considering ϵ to be small, we consider D to be large and write our solution as the following perturbation series:

$$C(r,z,t) = c_0(r,z,t) + D^{-1}c_1(r,z,t) + \cdots. \quad (7.1)$$

In this case, the leading two orders of (2.6) are

$$\nabla^2 c_0 = 0, \tag{7.2a}$$

$$\nabla^2 c_1 = \frac{\partial c_0}{\partial t}, \tag{7.2b}$$

where we use the ∇ notation because we want our discussion to be as general as possible. In addition, since the flux conditions all have $D(\partial C/\partial n)$ on the left-hand side, functionally they all become boundary conditions for c_1:

$$\frac{\partial c_0}{\partial n} = 0 \text{ at all boundaries}, \tag{7.3}$$

$$\frac{\partial c_1}{\partial z}(z=0) = 0, \qquad \frac{\partial c_1}{\partial z}(z=h_0) = -c_0(z=h_0)\frac{dh_0}{dt}, \tag{7.4a}$$

$$\frac{\partial c_1}{\partial r}(r=F) = \epsilon^2 k[c_0(r=F) - C_\infty], \qquad \frac{\partial c_1}{\partial r}(r=R) = Q_{\mathrm{w}}(c_0(r=R)). \tag{7.4b}$$

Here the second condition in (7.4a) comes from (3.12). The first condition in (7.4b) comes from (6.1b), and the second condition in (7.4b) comes from (3.6).

Solving (7.2a) subject to (7.3), we have that $c_0 = c_0(t)$ for any shape. Therefore, from (3.10) we have that to leading order, R is independent of z as well, so (4.7) holds. As a consequence, the volume of the domain of fluid is simply $h_0(t)S_h(t)$, where $S_h(t)$ is the surface area of the evaporating front at time t. In particular, in this domain we have $S_h = \pi(F^2 - R_0^2)$, as in the previous section.

Using this fact and integrating (7.2b) over the domain, we obtain

$$\begin{aligned} h_0(t)S_h(t)\frac{dc_0}{dt} &= \int_V \nabla^2 c_1 \, dV = \int_S \frac{\partial c_1}{\partial n} \, dS \\ &= S_h\left(-c_0\frac{dh_0}{dt}\right) + (2\pi F h_0)\epsilon^2 k(c_0 - C_\infty) - (2\pi R h_0)Q_{\mathrm{w}}(c_0), \end{aligned} \tag{7.5}$$

where we have used the Divergence Theorem. The first term comes from (7.4a) multiplied by the area of the surface over which it holds (S_h). Similarly, the remaining terms come from (7.4b) multiplied by the area of the surface over which they hold. Continuing to simplify, we have the following:

$$\begin{aligned} h_0\frac{dc_0}{dt} + c_0\frac{dc_0}{dt} &= \frac{2\pi F h_0}{S_h}\epsilon^2 k(c_0 - C_\infty) - \frac{2\pi R h_0}{S_h}Q_{\mathrm{w}}(c_0) \\ \frac{d(h_0 c_0)}{dt} &= \frac{S_F}{S_h}\epsilon^2 k(c_0 - C_\infty) - \frac{S_R}{S_h}Q_{\mathrm{w}}(c_0), \end{aligned} \tag{7.6}$$

where $S_R = 2\pi R h_0$ is the area of the surface at R, and similarly for S_F. If there is no flux out of the domain at either R or F, the right-hand side vanishes, and the total concentration

remains constant, as expected. The right-hand side is written in as general a form as possible, as discussed in more detail below. Equation (7.6) is coupled with (3.10) and (2.19), and our system becomes a more generalized version of the systems solved previously. In particular, we no longer have to solve a partial differential equation.

Things become more interesting if we think about coupling together a number of such subsystems. Assume we have a distribution of rods with radius $R^{(j)}(t)$ in domains of size $F^{(j)}$. In each the concentration is $c^{(j)}(t)$, with an overall concentration $C_\infty(t)$ in the liquid between them. The total concentration in the interstitial space changes through the boundaries at the $F^{(j)}$:

$$\frac{d(h_0 C_\infty)}{dt} = -\sum_j \frac{S_F^{(j)}}{S_\infty}(c^{(j)} - C_\infty), \tag{7.7}$$

where S_∞ is the surface area of the boundary to the interstitial space. Take the density of fibers to be n per unit area. Then $F \propto n^{-1/2}$. There should be a geometric argument to get the proportionality constant so that we have circles around each fiber and the remaining fluid as interstitial.

At this point, all the rod subproblems are the same, so it's really just two equations, one for c_0 and one for C_∞. An interesting complication to consider would be to construct a probability density function of initial radii $p(R(0))$, which obviously increases the dimensionality of the problem. One can work in this augmented space, solving one set of ODEs for each R_0 and producing means and variances of the corresponding solutions. Since this isn't a linear problem, Monte Carlo simulations would probably be needed to compute expectation values.

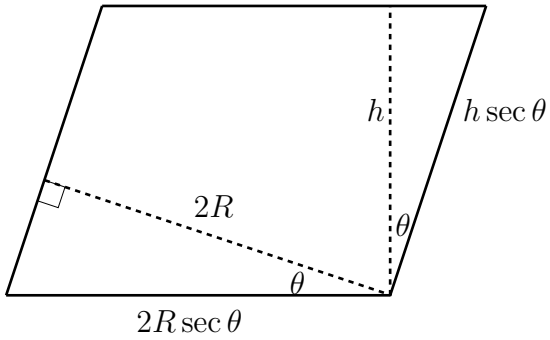

Figure 7.1: Cross section of oblique cylinder.

One could also think about the angle $\theta^{(j)}$ between each rod and the vertical. In the lumped formulation above, all that changes are the geometric factors, as shown in Fig. 7.1. In particular, the effective dimensions of the fiber are changed by a factor of $\sec\theta$. Hence if we still consider the full domain to be a right circular cylinder of radius F, then S_h becomes $\pi(F^2 - R^2\sec^2\theta)$, and S_R becomes $2\pi h_0 R\sec^2\theta$. One could then consider another probability density function $g(\theta)$ for the angle. The angle can't be too large or this model breaks down.

The basic rod-in-tube model with (r, z, t) dependence requires numerical solution as $R(t)$ evolves. There may be a way of obtaining a solution with fixed R and a moving upper

boundary using the "boost theorem" of [11], but the workshop ended before we had time to explore the idea fully.

Another possibility may be a reduced model in which the fibers are just treated as δ-function sinks for the flux:

$$\frac{\partial C}{\partial r}(r^{(j)}) = \delta(r - r^{(j)}) Q_{\mathrm{w}}(c_0^{(j)}), \tag{7.8}$$

where $r^{(j)}$ is the position of the jth fiber, with the usual boundary conditions on $z = 0$ and $z = h(t)$. This is a dilute model since it neglects the area taken up by the fibers, though that area can still be tracked using (3.10). There is still possible two-way coupling between the fluid and fibers depending on the form of Q_{w}. It might be possible to make analytical progress in the case of (3.13) and constant E, again using [11]. An open question is whether this would lead to a useful mean-field model based on the mean/statistical properties of the fiber distribution.

8 Homogenization for the Exterior Problem

We now adapt some relevant results from [14]. The authors consider a cleanup problem in which a cleanser interacts with an agent surrounding circular pore walls and removes the agent. (Similar modeling can be done when deposition happens around spherical nodes [12].) In our problem, deposition occurs on the outside of fibers that are taken to have circular cross-sections. We can adapt their work as follows.

In [14], two scales appear in the problem: a microscale corresponding to the thickness of the fibers, and a macroscale corresponding to the dimensions of the filter. Their ratio is taken to be a small parameter which we denote as δ, which means that on the filter spatial scale, the fibers are very small, which is similar to the δ-function approach in (7.8).

By choosing t_* to be the time scale corresponding to diffusion in the entire filter, we obtain $D = \delta^{-2}$ in our previous equations, which hold on the microscale. Hence as in Sec. 4, we find that the leading order of the concentration is independent of the microscale variables, and must be a function only of t and the macroscale variables. The approach is quite generic and can be adapted (theoretically at least) to any geometry.

In order to fully implement the method, one needs (a) a good 3D diffusion equation solver that can deal with a moving boundary in the vertical; and (b) a reliable solution for the unit cell (microscale) problem. Actually there may be decent approximations for the latter that would be good enough here, and a lookup table (offline) approach might be efficient and accurate enough. But quite a bit more work would be required to implement all of this.

For our reduced problem, it is enough to know that the homogenization process replaces the constant diffusion coefficient D with one that changes with the porosity of the matrix, which changes as $R(t)$ evolves. In general, D would be a tensor, but as we are considering diffusion only in the z-direction, we may treat D as a scalar.

Then using a similar notation to Sec. 3, the homogenized model reads

$$\frac{\partial}{\partial t}\left(V(R)C\right) = D\frac{\partial}{\partial z}\left(B(V(R))\frac{\partial C}{\partial z}\right) - L(R)Q_{\mathrm{w}}, \qquad \text{in} \quad 0 < z < h(t), \tag{8.1a}$$

$$C\frac{\mathrm{d}h}{\mathrm{d}t} = -DB(V(R))\frac{\partial C}{\partial z}, \qquad \text{at} \quad z = h(t), \tag{8.1b}$$

where B is a factor that relates the radius R (and hence the porosity of the matrix) to the diffusion coefficient. The other variables are as before. In particular, here Q_{w} is given by (3.13), and C is subject to the conditions in (2.12b). The evolution of $R(t)$ is governed by (6.5) and (3.11). For the evolution of the evaporation front $h(t)$, we use (3.14) subject to (2.12a).

From [5], we have that for a square lattice of fibers we can use

$$V(R) = 1 - (1 - V_0)R^2, \tag{8.2}$$

$$L(R) = 2\pi R, \tag{8.3}$$

$$B(V) = \frac{1}{1-V}\left(1 - \frac{2V}{1 + V - 0.3058V^4}\right), \tag{8.4}$$

where V_0 is the initial volume fraction. (Similar values can be found in [5] for a hexagonal lattice.)

To illustrate how the model behaves we ran simulations using a numerical scheme similar to the one described in Sec. 3.2. We show the results in Figs. 8.1–8.2, which show significant similarities with Figs. 3.1–3.3. Notice that in our case, as the material builds up around the fibers, the precipitate thickness is the variable R which is larger than one (which is the initial fiber radius).

Figure 8.1 shows the behavior of the system setting all the parameters to 1, except for the initial volume fraction which is set to 0.6 and 0.4 respectively. Compared to the results in a tube, the volume fraction appears as a new parameter of the system and, naturally, the lower the initial volume fraction the faster the clogging occurs. Apart from that, we observe very similar behavior to the tube model (Fig. 3.1), especially for the large initial volume fraction.

Looking at Fig. 8.2 we observe similar delaying effects when C_{sat} is larger than the initial concentration. Finally, Fig. 8.3 shows the effect of the diffusion coefficient in the system. Again, as it could be expected, faster diffusion delays the clogging.

In conclusion, this simple homogenized model captures the same features as the narrowing tube model posed in Sec. 3 but it introduces some new features such as the effect of the porosity (or volume fraction) in the model. These simulations could be easily extended for the hexagonal lattice, and with some extra work more complex geometries could be taken into account.

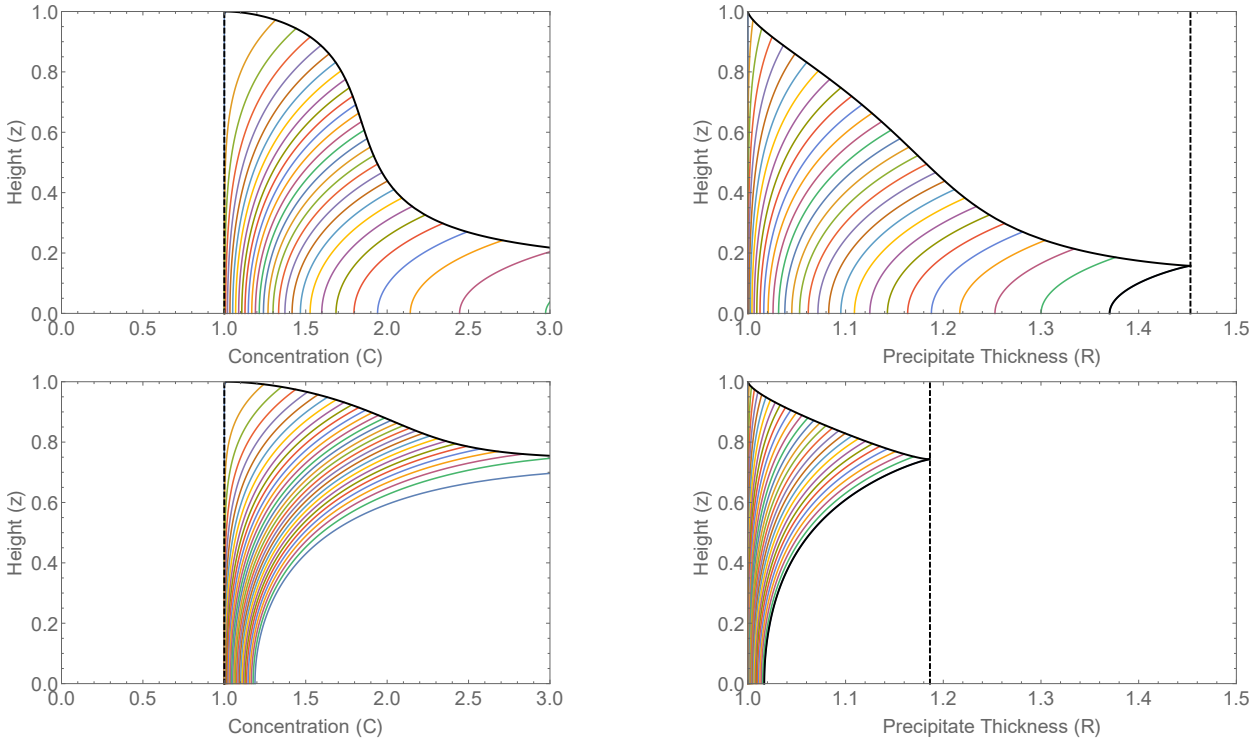

Figure 8.1: Comparison of effect of volume fraction on solution profiles. Diagrams are as in Sec. 3.2, with the addition of a dotted line on height graph indicating the line of symmetry where clogging will occur. All parameters equal to 1, except for initial volume fraction, which is 0.6 (top) and 0.4 (bottom).

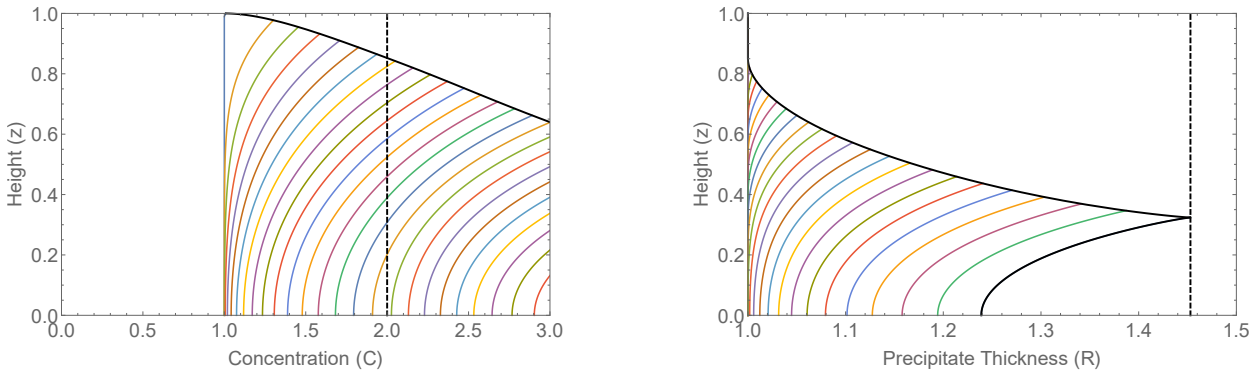

Figure 8.2: Comparison of effect of saturation on solution profiles. Parameters are as in the top figures in 8.1, except that $C_{\text{sat}} = 2$.

9 Additional Physical Considerations

In the previous sections, we presented only those models for surface adsorption and evaporation directly used in our solutions. In this section we present additional, more general

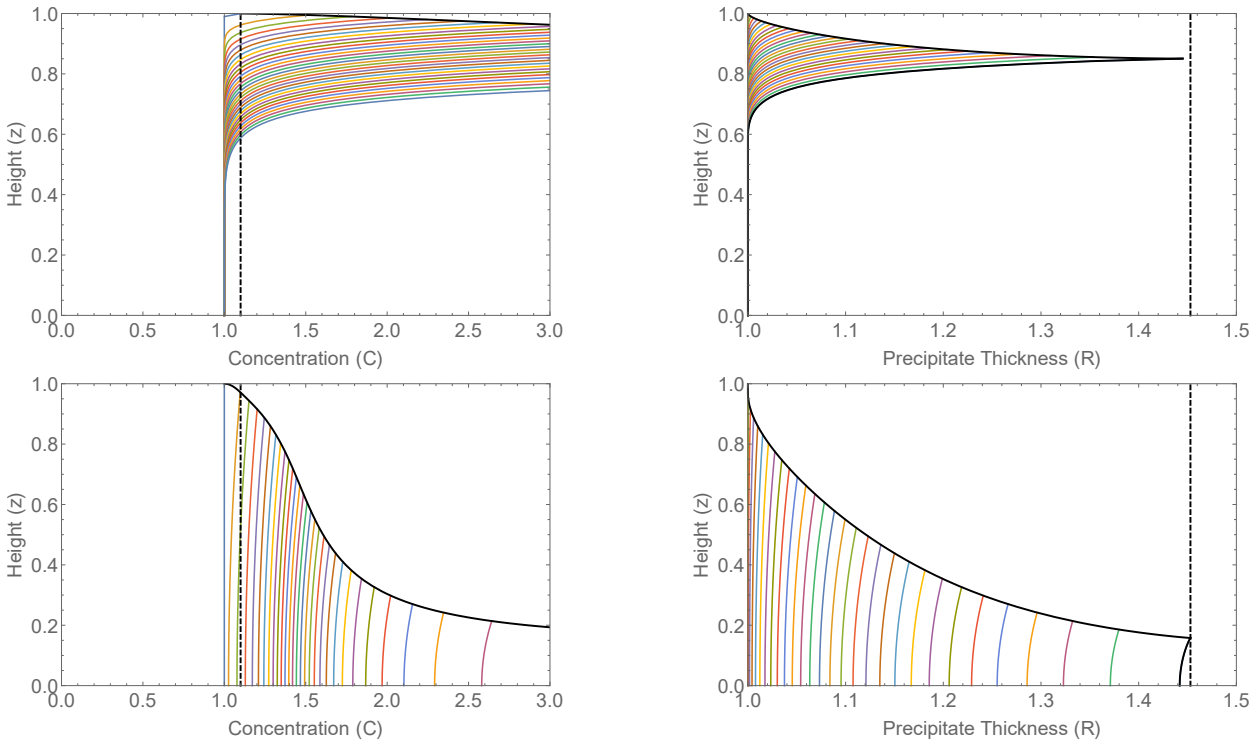

Figure 8.3: Comparison of effect of diffusion coefficient on solution profiles. Parameters are as in the top figures in 8.1, except that $C_{\text{sat}} = 1.1$, and $D = 0.1$ at top $D = 10$ at bottom.

models of some of the major additional effects that were deferred.

Specifically, the original problem description noted that the solute or solutes were surface active and, as such, adsorb to the liquid-gas interface. Moreover, at concentrations exceedng the critical micelle concentration, surfactant molecules can form micelles that likely also can precipitate onto the tube walls. It is also well-known that surfactant adsorption onto a liquid-gas interface can hinder liquid evaporation. This writeup extends the existing model to include descriptions of these additional issues.

Naturally there remain other issues that we do not take up in detail. For instance, if the aspect ratio of the pore is not small, the contact angle of the interface with the tube wall will come into play. In addition, there may be potential deposition from a contact line receding due to liquid evaporation.

9.1 Wall Dynamics

As discussed in Sec. 2.1, if the solute is taken to be surface active, then a simple model for adsorption is given by the Langmuir isotherm (2.17), which we further simplified using the linear relation (2.18).

One can easily change the choice of isotherm should data from Gore suggest that another isotherm describes the surfactant's interaction with the interface better. For instance, one

can use the Frumkin model, which is given by (in our notation)

$$\frac{\Gamma e^{-A\Gamma}}{1-\Gamma} = KC, \tag{9.1}$$

where we have dropped the dot subscripts for simplicity. (Here we have taken the equilibrium value of $\Gamma = 1$ because of the normalization we used.) Note that if we take $A = 0$, then we have

$$\Gamma = KC(1-\Gamma)$$
$$\Gamma = \frac{KC}{1+KC},$$

which is exactly (2.17).

Also note that in Sec. 2, we did not model narrowing of the pore by adsorption, and the narrowing we did discuss in Sec. 3 was assumed to follow a different mechanism. If we do allow pore narrowing due to surface adsorption, we would simply replace $Q_{\rm w}$ by $\partial\Gamma_{\rm w}/\partial t$ in (3.10), yielding

$$\frac{\partial\tilde{R}}{\partial\tilde{t}} = -\tilde{\chi}\frac{\partial\tilde{\Gamma}_{\rm w}}{\partial\tilde{t}}, \tag{9.2}$$

where $\tilde{\chi}$ can now be interpreted as the size added to the wall per adsorbed surfactant molecule.

Note that (2.17) and (9.1) are equilibrium models: in other words, Γ instantly equilibrates with the value of C just inside the interface. In actuality, there is a time scale on which the surfactant achieves a local equilibrium distribution (*i.e.*, isotherm) between its surface concentration and that bulk concentration immediately inside the interface. Hence we have implictlly assumed that this time scale is much shorter than the time for interface motion and for bulk concentration variation in the interface sublayer.

If instead the time scale for adsorption is similar to bulk diffusion, then we would have to track the evolution of Γ directly; one nonequilibrium version is given by [6]

$$\frac{\partial\Gamma}{\partial t} = e^{-A\Gamma^2}[KC(1-\Gamma) - \Gamma e^{-A\Gamma}],$$

the steady state of which is given by (9.1). Taking $A = 0$ in the above, we obtain

$$\frac{\partial\Gamma}{\partial t} = KC(1-\Gamma) - \Gamma, \tag{9.3}$$

the steady state of which is given by (2.17). The form (9.3) provides fuller physical insight into our models for wall dynamics.

In particular, the Langmuir and Frumkin isotherm models describe rapid equilibration of the adsorption of a surfactant molecule to a surface site (first term on the right-hand side) and its desorption from the same surface site (second term). This analysis is subject to the caveat that the total number of surface sites for adsorption (those with plus those without

a molecule of adsorbed surfactant) is fixed and fairly small. Thus the number of free sites changes appreciably with time [$(1-\Gamma)$ term in (9.3)].

Though the Langmuir isotherm works well for adsorption at the interface, upon further reflection we realized that wall deposition is more complicated. First, wall deposition happens on a slow time scale, which is inconsistent with the rapid equilibrium of the isotherm models. Hence using an equation similar to (9.3) made more sense.

We also assumed that deposition would be irreversible (which would imply ignoring the second term on the right-hand side of (9.3)), and that the number of wall surface sites is so large that the number occupied is negligible (which would imply replacing the first term with KC). In that case, keeping in mind that $Q_{\rm w}$ and $\partial\Gamma/\partial t$ play similar roles, we obtain an equation very similar to (3.13).

9.2 Evaporation

Though in (2.19) we postulated that the evaporation rate may depend on concentration, for our simulations we used (3.14), which has a constant evaporation rate. However, even in the case where E is independent of concentration, it may still depend on the drying temperature. It may also depend on the humidity differential, which may change over the course of the drying due to changes in C at the interface.

It has been well known since a 1925 paper [17] that a surfactant monolayer can inhibit the evaporation of liquids like water. Literature focusing on liquid layers heated from below (not our interest) identifies a significant lowering of the evaporation due to the inherent resistance to evaporation of the surfactant layer itself.

Plots that summarize experiments typically use the ratio $E_{\rm clean}/E_{\rm surfactant}$ of clean surface to surfactant-loaded surface evaporation rates as the dependent variable. We have found two types of relevant data sets (e.g., [1]). In the first, the logarithm of the ratio of evaporation rates is exponential in the surfactant concentration Γ_h. In the second, the logarithm of the ratio of evaporation rates is found to be nearly linear in the surface pressure, defined as the difference between the surface tensions σ of the clean and surfactant-laden interfaces. These trends are similar but not identical.

In order to analyze the variation with surface pressure, we find data suggesting that, for many surfactants, the change in the ratio $(\sigma_{\rm surfactant}/\sigma_{\rm clean})$ of the surface tension of the surfactant-laden to that of the clean surface with increasing bulk concentration C is nearly flat at one for small bulk concentrations and then turns into a decline that is proportional to $-\ln C$ and persists until the critical micelle concentration or CMC. If we approximate this curve by two straight lines that intersect at a concentration C_*, then we can approximate the data by

$$\frac{\sigma_{\rm surfactant}}{\sigma_{\rm clean}} = \begin{cases} 1, & 0 < C < C_*, \\ 1 - \ln\frac{C}{C_*}, & C_* < C < C_{\rm CMC}. \end{cases} \tag{9.4}$$

Combining this relation with the the given exponential decay of the ratio of evaporation

rates with the surface pressure, one easily finds

$$\frac{E_{\text{surfactant}}}{E_{\text{clean}}} = \left(\frac{C}{C_*}\right)^{-b} \qquad \Longrightarrow \qquad E(t) = E_{\text{clean}} \left(\frac{C}{C_*}\right)^{-b}, \tag{9.5}$$

where b is the slope of the $\ln(E_{\text{clean}}/E_{\text{surfactant}})$ *vs.* surface pressure curve, and we have used the fact that in our notation, $E_{\text{surfactant}}$ is the evaporation rate $E(t)$.

Alternatively, if one combines an exponential growth of $E_{\text{clean}}/E_{\text{surfactant}}$ as a times the surfactant concentration Γ_h with the Langmuir isotherm, one gets

$$\frac{E_{\text{surfactant}}}{E_{\text{clean}}} = \exp\left(-a\frac{K_h C}{1+K_h C}\right) \qquad \Longrightarrow \qquad E(t) = E_{\text{clean}} \exp\left(-a\frac{K_h C}{1+K_h C}\right). \tag{9.6}$$

Both of these equations give similar dependences over a regime of C not too large, and both can be used in (2.19) to track $h(t)$.

A final note: the vapor pressure of a mixture of water and a non-volatile solute is proportional to the mole fraction of water. So, as long as the solute does not appreciably change the mole fraction of water, the vapor pressure remains essentially unchanged.

9.3 Micelles

When its concentration exceeds a critical micelle concentration C_{CMC}, the surfactant can form micelles that can also dissolve back into individual surfactant molecules. We model this process by a simple mass action kinetic equation. Let M be the (dimensionless) concentration of micelles, which we assume each to be comprised of N surfactant molecules. Then we find the net (dimensionless) rates of change, f_M of micelle concentration and f_C of monomer surfactant molecules, due to reaction, are

$$f_M = k_{\text{a}}(C - C_{\text{CMC}})^N - k_{\text{d}} M = -\frac{f_C}{N}, \tag{9.7}$$

where k_{a} and k_{d} are the association and dissociation rate constants, respectively. Here the factor of N is due to the fact that N surfactant molecules must combine to form a micelle. This new rate of change may be added directly to (3.9) to yield

$$\frac{\partial(C_0[R(z,t)]^2)}{\partial t} = D\frac{\partial}{\partial z}\left([R(z,t)]^2\frac{\partial C_0}{\partial z}\right) - 2R(z,t)Q_{\text{w}}(C_0) - N[R(z,t)]^2 f_M, \tag{9.8}$$

where the R^2 term arises from the fact that micelle formation occurs throughout the domain.

These micelles can also precipitate out of solution onto the walls at a rate Q_M. The equations for surfactant precipitation assume that the concentration of surfactant in the liquid at the wall is C_{sat} and that of the micelles is zero, meaning that as soon as a micelle reaches the wall, it precipitates. Both equations assume that the rate of precipitation onto the wall is fast compared with sublayer diffusion and thus sublayer diffusion controls the overall rate.

Given these facts, we see that the evolution equation for M is quite similar to (9.8):

$$\frac{\partial(M[R(z,t)]^2)}{\partial t} = D_M \frac{\partial}{\partial z}\left([R(z,t)]^2 \frac{\partial C_0}{\partial z}\right) - 2R(z,t)Q_M(M) + [R(z,t)]^2 f_M. \tag{9.9}$$

It is reasonable to assume that in solution both the surfactant and the micelle are roughly spherical. In that case we may use the Stokes-Einstein relation, which states that the molecular diffusivity is inversely proportional to the molecular radius, to obtain $D_M = D/N^{1/3}$.

We assume that initially there are no micelles, and the symmetry condition at $z = 0$ must also hold:

$$M(z,0) = 0, \qquad \frac{\partial M}{\partial z}(0,t) = 0.$$

It is reasonable to assume that micelles don't adsorb to the interface, but first decompose in the liquid since there is no indication that micelles exist on the interface. This is because a micelle exists in order for ampiphillic molecules to shield their hydrophobic potions from the aqueous environment; at the interface, the interface itself does that. Hence the evaporation front condition for M is similar to (3.12), where we assumed no adsorption:

$$D_M \frac{\partial M}{\partial z}(h_0(t),t) + M(h(t))\frac{dh}{dt} = 0. \tag{9.10}$$

We may also postulate a constitutive equation analogous to (3.13) for deposition of micelles:

$$Q_M = \lambda_M M, \tag{9.11}$$

with a new mass transfer coefficient λ_M replacing λ. These coefficients are each presumed to represent the ratio of the molecular diffusivity to the thickness of a diffusive sublayer for each species adjacent to the wall. It is reasonable to assume that the thickness of this sublayer is similar for surfactant molecules and for micelles. In that case we may also use the Stokes-Einstein relation to obtain $\lambda_M = \lambda/N^{1/3}$. The expression for Q_M assumes that only single surfactant molecules and not micelles desorb from the wall.

Since there are now two deposition mechanisms, (3.10) would be replaced by

$$\frac{\partial R}{\partial t} = -\chi(Q_{\mathrm{w}} + NQ_M),$$

with the extra factor of N due to the fact that each micelle contributes N molecules to the layer.

Many of the parameters of the original MPI model were estimated during the MPI. The few additional unknown parameters for micelle formation and retardation of the evaporation rate herein await further input from Gore.

Nomenclature

Units are listed in terms of length (L), moles (N), and time (T). If a symbol appears both with and without tildes, the symbol with tildes has units, while the one without is dimensionless. Equation numbers where a variable is first defined is listed, if appropriate.

A: dimensionless constant in Frumkin model (9.1).
a: decay constant in evaporation model (9.6).
B: factor relating diffusion coefficient to porosity (8.1a).
b: decay exponent in evaporation model (9.5).
$\tilde{C}(\tilde{r},\tilde{z},\tilde{t})$: volume concentration of particle in pore, units N/L^3 (2.1).
$\mathcal{C}$: expansion of C for small D and ϵ (4.1).
c: expansion of C for small D (7.1).
$\tilde{D}$: diffusion coefficient, units L^2/T (2.1).
$\tilde{E}$: evaporation rate, units L/T (2.19).
F: far-field radius, dimensionless (6.1a).
f: dimensionless rate of change of concentration due to micelle formation (9.7).
$g(\theta)$: proposed probability density function for θ.
H: maximum height of pore, units L (1.2).
$\tilde{h}(\tilde{r},\tilde{t})$: evaporation front, units L (1.1).
j: indexing variable (7.7).
K: dimensionless equilibrium constant (2.17).
k: dimensionless constant relating bulk and boundary concentration (2.9) or dimensionless rate constant (9.7).
M: dimensionless micelle concentration (9.7).
N: number of molecules per micelle (9.7).
n: fiber density.
p: probability density function for initial radii.
$\tilde{Q}_{\mathrm{w}}$: deposition flux, units N/L^2T (3.1).
R: radius of pore, variously defined (1.1).
$\tilde{r}$: radial variable in pore, units L (1.1).
S: surface (7.5).
$\tilde{t}$: time variable, units T (1.1).
V: volume (8.1a).
$\mathcal{Z}$: the integers.
$\tilde{z}$: height variable in pore, units L (2.1).
α: surplus of the contact angle over $\pi/2$ (1.1).
β: constant in large-D solution (4.5).
δ: ratio of length scales in homogenization problem.
$\tilde{\Gamma}$: area concentration, variously defined, units N/L^2 (2.2).
ϵ: small aspect ratio (1.3).
θ: angle of fibrous rod with vertical.
$\tilde{\lambda}$: coefficient in precipitation constitutive law, units L/T (3.13).
σ: surface tension (9.4).
$\tilde{\chi}$: constant relating wall growth to precipitation flux, units L^3/N (3.2).

Other Notation

a: as a subscript on k, refers to association (9.7).
C: as a subscript, refers to bulk concentration (9.7).
c: as a subscript on t, refers to the clogging time.
d: as a subscript on k, refers to dissociation (9.7).
CMC: as a subscript on C, refers to the critical micellular concentration.
F: as a subscript on S, used to refer to the outer surface (7.6).
H: as a subscript on ∇, used to refer to horizontal derivatives (8.1a).
h: as a subscript, used to refer to the evaporation front (2.13).
i: as a subscript, refers to the initial condition (2.3).
$j \in \mathcal{Z}$: as a subscript, used to refer to a perturbation series (1.4). As a superscript, used to refer to a fiber (7.7).
M: as a subscript, refers to micelles (9.7).
R: as a subscript on S, used to refer to the inner surface (7.6).
sat: as a subscript, refers to a saturation value (3.13).
T: as a subscript on Γ, used to refer to a total number of adsorption sites (2.5b).
w: as a subscript, used to refer to the pore wall (1.1).
∞: as a subscript, refers to a far-field condition (6.1b).
$*$: as a subscript, refers to a characteristic value (2.5a).
$\langle\cdot\rangle$: cross-sectional average (2.16).
$\hat{}$: refers to an expansion for large λ (5.2).

References

[1] Barnes, G.: The effects of monolayers on the evaporation of liquids. Advances in Colloid and Interface Science **25**, 89–200 (1986)

[2] Breward, C., Howell, P.: Straining flow of a micellar surfactant solution. Euro. J. Appl. Math. **15**(5), 511–531 (2004)

[3] Breward, C.J., Howell, P.: Modeling surfactant systems out of thermodynamic equilibrium. SIAM J. Appl. Math. **79**(3), 1098–1123 (2019)

[4] Breward, C.J.W., Griffiths, I.M., Howell, P.D., Morgan, C.E.: Straining flow of a weakly interacting polymer-surfactant solution. Euro. J. Appl. Math. **26**(5), 743–772 (2015)

[5] Bruna, M., Chapman, S.J.: Diffusion in spatially varying porous media. SIAM Journal on Applied Mathematics **75**(4), 1648–1674 (2015)

[6] Chomaz, J.M.: The dynamics of a viscous soap film with soluble surfactant. Journal of Fluid Mechanics **442**, 387–409 (2001)

[7] Edmonstone, B.D., Craster, R.V., Matar, O.K.: Surfactant-induced fingering phenomena beyond the critical micelle concentration. J. Fluid Mech. **564**, 105–138 (2006)

[8] Edwards, D., Brenner, H., Wasan, D.: Interfacial transport processes and rheology. Butterworth-Heinemann (1991)

[9] Hennessy, M.G., Breward, C.J.W., Please, C.P.: A two-phase model for evaporating solvent-polymer mixtures. SIAM J. Appl. Math. **76**(4), 1711–1736 (2016)

[10] Kaplan, C.N., Mahadevan, L.: Evaporation-driven ring and film deposition from colloidal droplets. J. Fluid Mech. **781** (2015)

[11] King, M.J.: Immiscible two-phase flow in a porous medium: Utilization of a laplace transform boost. Journal of mathematical physics **26**(4), 870–877 (1985)

[12] Kiradjiev, K.B., Breward, C.J.W., Griffiths, I.M., Schwendeman, D.: A Homogenised Model for a Reactive Filter. SIAM J. Appl. Math. (2020). *Under Review*

[13] Kiradjiev, K.B., Nikolakis, V., Griffiths, I.M., Beuscher, U., Venkateshwaran, V., Breward, C.J.W.: A Simple Model for the Hygroscopy of Sulfuric Acid. Ind. & Eng. Chem. Res. **59**(10), 4802–4808 (2020)

[14] Luckins, E., Breward, C., Griffiths, I., Wilmott, Z.: Homogenisation problems in reactive decontamination. European Journal of Applied Mathematics pp. 1–24 (2019)

[15] Morgan, C.E., Breward, C.J.W., Griffiths, I.M., Howell, P.D.: Mathematical modelling of surfactant self-assembly at interfaces. SIAM J. Appl. Math. **75**(2), 836–860 (2015)

[16] Perez, E.B., Carvalho, M.S.: Drying of thin films of polymer solutions coated over impermeable substrates. Heat Transfer Engineering **28**(6), 559–566 (2007)

[17] Rideal, E.K.: On the influence of thin surface films on the evaporation of water. The Journal of Physical Chemistry **29**(12), 1585–1588 (1925)

[18] Shokri, N., Or, D.: What determines drying rates at the onset of diffusion controlled stage-2 evaporation from porous media? Water Resources Research **47**(9) (2011)

[19] Willmott, G.R., Neto, C., Hendy, S.C.: Uptake of water droplets by non-wetting capillaries. Soft Matter **7**(6), 2357–2363 (2011)

A Appendix

A typical pore has radius $R = 5\,\mu$m, while it has a typical length of $H = 100\,\mu$m.

We have parameter values of

$$\tilde{D} = \frac{10^{-10}\ \mathrm{m}^2}{\mathrm{s}}, \tag{A.1}$$

$$\tilde{E} = \frac{5\ \mathrm{g\ H_2O}}{\mathrm{m}^2 \cdot \mathrm{min}} \left[\frac{10^{-6}\ \mathrm{m}^3 \cdot \mathrm{min}}{\mathrm{g}(60\ \mathrm{s})}\right] = 8.33 \times 10^{-8}\, \frac{\mathrm{m}}{\mathrm{s}}. \tag{A.2}$$

Note that if we choose $t_* = H/\tilde{E}$ as discussed below (2.19), then

$$D = \frac{\tilde{D}}{\tilde{E}H} = \frac{10^{-10}}{(8.33 \times 10^{-8})(10^{-4})} = 12,$$

which might be large enough to do some large-D asymptotics.

The CMC limit is supposed to be

$$C_{\mathrm{CMC}} = 5 \times 10^{-4} \frac{\mathrm{mol}}{\mathrm{L}}. \tag{A.3}$$

The initial volume concentrations will be around

$$C_{\mathrm{i}} = 10^{-7} \frac{\mathrm{mol}}{\mathrm{L}}. \tag{A.4}$$

The maximum surface pore concentration will be around

$$\Gamma_{\mathrm{w,T}} = 1.02 \times 10^{-7}\, \frac{\mathrm{mol}}{\mathrm{m}^2} \tag{A.5}$$

This assumes a radius of 1 nm, and 74% of the surface area is covered. We may use the same value for $\Gamma_{h,\mathrm{T}}$.

Note that these values make k_{w} large:

$$k_{\mathrm{w}} = \frac{2(1.02 \times 10^{-7}\,\mathrm{mol/m^2})}{(10^{-7}\mathrm{mol/L})(5 \times 10^{-6}\ \mathrm{m})} = \frac{(0.408 \times 10^{6})(10^{-3}\ \mathrm{m}^3)}{\mathrm{m}^3} = 408. \tag{A.6}$$

However, since the K values are unknown, they may be small enough to generate the balance needed in the narrowing section.

Porous Media Subgroup Report

B.S. Tilley
Worcester Polytechnic Institute

Philip Broadbridge
La Trobe University

June 18, 2020

We are interested in finding the deposition concentration of soluble surfactants (monomers) along with micelle concentrations within a saturated porous membrane as the solvent evaporates isothermally. Note that the thickness of the membrane (approximately 100 μm) is comparable to the typical pore size (approximately 10 μm), so the porous medium approach described here should be viewed as a crude approximation to the solute and moisture dynamics within the membrane. A representative elementary volume with diameter covering the membrane thickness would still barely cover a representative sample of pore sizes. A spatial sequence of such sample volumes could reasonably represent a medium that was 10 times thicker (*i.e.*, at least at the millimeter scale.) Given the thinness of the layer compared to the typical spanwise lengths of the membrane, the evolution equations discussed here consist of a single spatial dimension corresponding to the thickness direction.

We model the flow within the membrane as a porous medium flow, with porosity θ_s throughout the membrane. In addition, we assume that the porosity does not change over time as the species deposits upon the membrane matrix. Hydrostatic pressures in this film are assumed to be negligible, and the dynamics of the flow are driven primarily by capillary pressure. Over a representative volume, this flow can be represented in terms of the moisture content of the membrane. The moisture dynamics are governed by the continuity equation

$$\frac{\partial \theta}{\partial t} + \frac{\partial q}{\partial z} = 0, \tag{1}$$

where $0 \leq \theta \leq \theta_s < 1$ is the volumetric moisture content of the porous medium, θ_s is the maximum moisture content, corresponding to the porosity of the medium, and q is the Darcy flux within the medium. Since hydrostatics are assumed to be negligible compared to capillary-driven flows, the Darcy flux is given by

$$q = K(\theta)\Psi'(\theta)\frac{\partial \theta}{\partial z} = -D_w(\theta)\frac{\partial \theta}{\partial z}, \tag{2}$$

where $K(\theta) = k(\theta)\,\rho\,g/\mu$ is the scaled permeability of the porous medium, μ is the fluid dynamic viscosity, Ψ is the capillary head, or the capillary pressure divided by the specific weight of the fluid. These topics can be described in more detail in Bear's text [1], along with the paper by Stewart & Broadbridge [2]. D_w needs to be positive, strictly increasing and its rate is also strictly increasing ($D_w > 0, D'_w > 0$, and $D''_w > 0$). Formally, we follow [2] and use the form

$$D_w = \frac{a}{(b-\theta)^2}\ ,$$

for convenience. This choice gives an integrable model for the nonlinear diffusion equation that can be transformed to the linear diffusion equation and solved, subject to standard boundary conditions. For porous media, b/θ_s is typically between 1.05 and 1.2, and a is the characteristic dimensional value of D_w. In this report, we set $b = 1$ for convenience [3].

The continuity equation simplifies to

$$\frac{\partial\theta}{\partial t} = \frac{\partial}{\partial z}\left\{D_w(\theta)\,\frac{\partial\theta}{\partial z}\right\}\ ,\ t > 0\ ,\ 0 < z < H, \tag{3}$$

where H is the half-thickness of the membrane.

The dynamics of the flow in the membrane are driven by evaporation, and there are two distinct stages of evaporation that have been described for soils. The first stage corresponds to a constant evaporation rate at the surface of the porous medium. In this stage, the atmospheric kinetics control the evaporation rate. In the second stage, which represents a falling evaporation rate, percolation of the flow within the porous medium is the limiting factor in the removal of water through evaporation. These stages can be represented in terms of the relative humidity h. Stage 1 evaporation corresponds to $h \approx 1$ while evaporation for stage 2 corresponds to $h < 1$.

To model the absorption-desorption processes for the surfactant, we consider a model by Rosen [4] which captures the rate of the total concentration c which is mass of transported material (both mobile dissolved component and immobile component) per unit volume of water content as a result of diffusion and convection. In the fluid phase

$$\frac{\partial c}{\partial t} + \mathbf{v}\cdot\nabla c_m = \mathcal{D}\,\nabla^2 c_m\ , \tag{4}$$

where $\mathbf{v}$ is a prescribed velocity, $\mathcal{D}$ is the diffusion constant of the species, and $c_m = c_s\,c/(c_s + c)$ is the mobile concentration of the surfactant within the solution. c_s is the maximum concentration possible within the solvent. Michaelis-Menten kinetics are assumed to take place at a much faster rate than diffusion or advection in this model. If precipitation is bimolecular and solution is monomolecular, then $c_m c = c_s(c - c_m)$ where c_m is the concentration of mobile component in solution and $c - c_m$ is the precipitate concentration, c is the total gravimetric concentration and c_s is a constant that is interpreted as maximum saturated level of dissolved solute. Then it follows that

$$c_m(x,t) = \frac{c}{1 + c/c_s} \quad \to \quad c_s, \quad c \to \infty, \tag{5}$$

$$\sim \quad c, \quad c \to 0. \tag{6}$$

Extending this model to our porous medium (e.g. see [5] for a non-reacting species example) gives

$$\frac{\partial\,(\theta\,c)}{\partial t} - \frac{\partial}{\partial z}\left[D_w(\theta)\frac{\partial\theta}{\partial z}\,c_m\right] = \frac{\partial}{\partial z}\left[D^*\,\theta\,\frac{\partial c_m}{\partial z}\right]\ , \tag{7}$$

where D^* here is the dispersivity (see [5]). Note that the water concentration θ is volume of water per unit volume of total porous material mixture, whereas c is the mass of transported species per unit volume of water, and concentration θc is the mass of transported species per unit volume of porous material mixture.

To determine the immobile species concentration based on volume of mixture, we look at the remaining components after eliminating the mobile component as

$$\theta c_{im} = \theta\,(c - c_m)\ . \tag{8}$$

Note that this formulation automatically accounts for the deposited immobile component. However after extensive drying, the species concentration will be largely the immobile component which is a small concentration of water θ multiplying a large concentration c_{im} based on a small water volume. Finally, for this problem we expect that the evaporation rate is relatively slow compared to the porous medium flow. This suggests that stage 1 for evaporation only, and our boundary conditions for the problem are symmetry conditions along $z = 0$, and evaporation and no species flux conditions along $z = H$:

$$\underline{z = 0}: \qquad \frac{\partial\theta}{\partial z} = \frac{\partial c}{\partial z} = 0\ , \tag{9}$$

$$\underline{z = H}: \qquad -D_w(\theta)\frac{\partial\theta}{\partial z} = R^*\ , \tag{10}$$

$$D_w(\theta)\frac{\partial\theta}{\partial z}\,c_m + \theta\,D^*\,\frac{\partial c_m}{\partial z} = 0\ . \tag{11}$$

Finally we assume that the membrane is initially fully saturated and has a uniform monomer distribution

$$\theta(z,0) = \theta_s\ ,\ c(z,0) = c_i^*\ . \tag{12}$$

Before developing a computational approach to solve (3), (7) subject to boundary conditions (9), (10), and (11) and initial conditions (12), we apply nondimensionalization. We scale species concentration on the largest mobile concentration c_s, z on the half-thickness of the membrane H, and t on the Darcy-flow time scale H/a, where a is the value of diffusivity at low moisture content. With this choice of scales, $H \approx 10^{-4}$ m, $a \approx 10^{-11}\,\mathrm{m}^2/\mathrm{s}$ and $H/\bar{a} \approx$ 17 min. The characteristic time for the membrane to dry in Gore's experiments is around 33 min, so we are concerned in this problem with $0 < t < 2$ approximately. Applying these

scales to our system we find

$$\frac{\partial \theta}{\partial t} = \frac{\partial}{\partial z}\left\{ D_w(\theta)\,\frac{\partial \theta}{\partial z} \right\} \ , \ t > 0 \ , \ 0 < z < 1, \tag{13}$$

$$\frac{\partial\,(\theta\, c)}{\partial t} - \frac{\partial}{\partial z}\left[D_w(\theta)\frac{\partial \theta}{\partial z}\, c_m \right] = \frac{\partial}{\partial z}\left[D\,\theta\,\frac{\partial c_m}{\partial z} \right] \ , \tag{14}$$

$$\underline{z = 0}: \qquad \frac{\partial \theta}{\partial z} = \frac{\partial c}{\partial z} = 0 \ , \tag{15}$$

$$\underline{z = H}: \qquad -D_w(\theta)\frac{\partial \theta}{\partial z} = R \ , \tag{16}$$

$$D_w(\theta)\frac{\partial \theta}{\partial z}\, c_m + \theta\, D\,\frac{\partial c_m}{\partial z} = 0 \ , \tag{17}$$

$$\underline{t = 0}: \qquad \theta(z,0) = \theta_s \ , \ c(z,0) = c_i \ , \tag{18}$$

where the nondimensional reaction parameter $R = R^* H/a$, and the scaled dispersivity $D = D^*/a$.

To computationally model (13)–(18), we apply finite differences in space, and a full Crank-Nicholson formulation in time. Since the moisture content θ is decoupled from the species, we solve (13) first, and then use this data to solve for the monomer species concentration. For (14), we solve for c_m directly using the nondimensional definition for c_m

$$c = \frac{c_m}{1 - c_m} \ .$$

The simulation continues until the surface moisture content reaches a small and finite value. Note that $\theta \to 0$ is a singular limit in the species equation, and we expect θ to reach zero first at $z = 1$. In the solutions which follow, we stop the simulation when $\theta(1,t) < \Delta z$, where Δz is the spatial mesh spacing.

From the given time scale, we can calculate an estimate of the nondimensional evaporation coefficient, which then provides a single parameter to explore, being the nondimensional dispersivity D. We use the moisture content equation to find an R where dryout occurs near t = 2. Then we explore immobile surfactant distributions based on dispersivity. A good estimate appears to be $R = 0.25$, as is shown in Figure 1, where we have chosen $\theta_s = 0.6$ based on Gore's values for the membrane porosity. Note that the final moisture content at the end of this stage is below 20 %.

The monomer distribution during the removal of solvent from the membrane depends significantly on the dispersivity parameter D. In Figure 2 we consider the evolution of the mobile component (Figure 2a) and the immobile component (Figure 2b). We note that the concentration of each component increases over time, as would be expected since the volume of solvent is decreasing over evaporation. For later times, however, we note the increase in concentration near the membrane surface.

While the immobile species concentration increases near the membrane surface at the end of stage 1 for $D = 1$, Figures 3 and 4 show different species evolution of the mobile and immobile components for $D = 4$ and $D = 8$, respectively. For $D = 4$ in Fig. 3, the

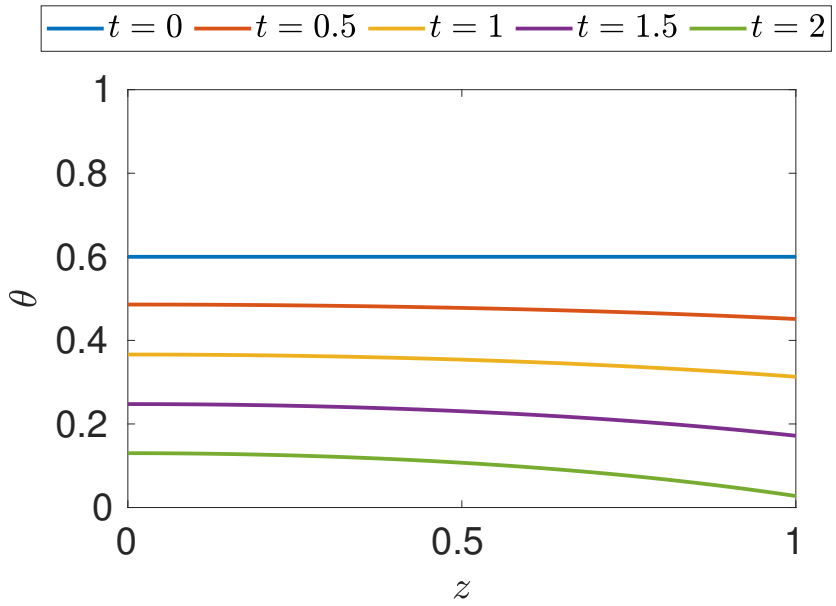

Figure 1: Evolution of moisture content over the membrane half-thickness $0 < z < 1$ for $R = 0.25$, $\theta_s = 0.6$, and $D = 1$ at nondimensional times $t = 0, t = 0.5, t = 1, t = 1.5, t = 2$.

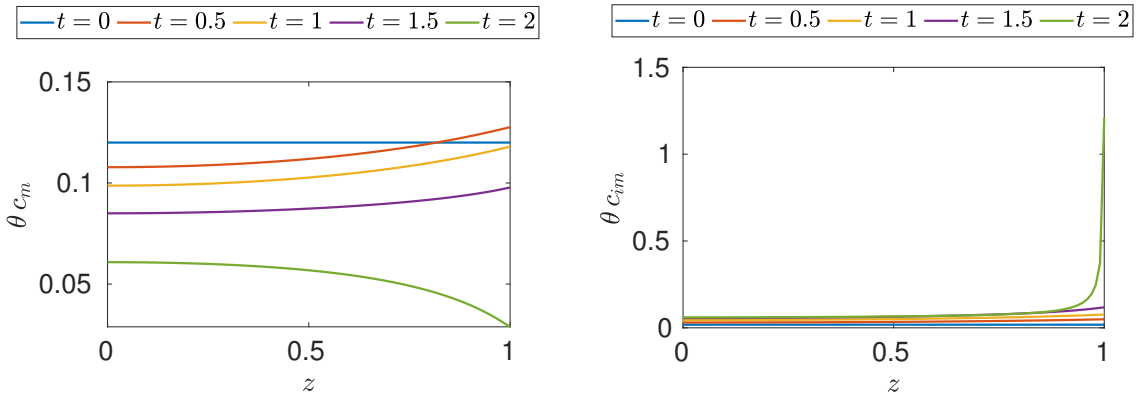

(a) (b)

Figure 2: Evolution of monomer surfactant concentration for $R = 0.25$, $\theta_s = 0.6$, and $D = 1$ at times $t = 0$, $t = 0.5$, $t = 1$, $t = 1.5$, and $t = 2$ for (a) mobile species, and (b) immobile species.

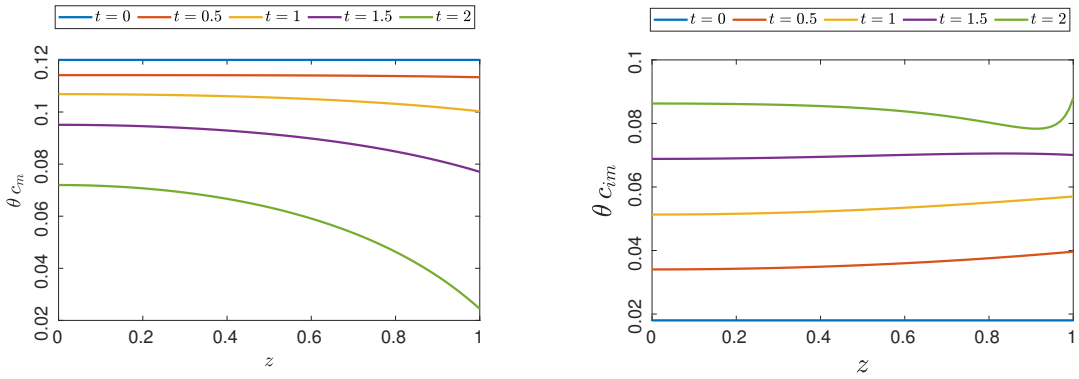

(a) (b)

Figure 3: Evolution of monomer surfactant concentration for $R = 0.25$, $\theta_s = 0.6$, and $D = 4$ at times $t = 0$, $t = 0.5$, $t = 1$, $t = 1.5$, and $t = 2$ for (a) mobile species, and (b) immobile species.

steady decrease in the mean of the mobile component is balanced by the steady increase in the immobile component. However, near the time of the loss of moisture on the membrane surface, we see that the spatial variation of the immobile component is relatively uniform throughout the domain, with a slight build-up of the species near the membrane surface. Note that the centerline values of $\theta\, c_{im}$ are similar at $z = 0$ and $z = 1$.

For $D = 8$, we find that the immobile component at the later stages of the simulation is *reduced* near the membrane surface but *increases* more rapidly near the centerline. This qualitatively agrees with the reports on experiments from Gore where for some cases a film of surfactant remained near the membrane surface (in our case, $D = 1$), while other cases resulted in the immobile component remaining within the bulk of the membrane ($D = 8$).

References

[1] J. Bear. *Dynamics of Fluids in Porous Media*. Dover, 1988.

[2] J.M. Stewart and P. Broadbridge. Calculation of humidity during evaporation from soils. *Adv. Water Res.*, 22(5):495–505, 1999.

[3] A. Warrick. *Soil Water Dynamics*. Oxford Univ. Press, 2003.

[4] G. Rosen. Method for the exact solution of a nonlinear diffusion-convection equation. *Phys. Rev. Lett.*, 49:1844–1847, 1982.

[5] R.J. Moitsheki, P. Broadbridge, and M.P. Edwards. Symmetry solutions for transient solute transport in unsaturated soils with realistic water profile. *Trans. Porous Media*, 61(1):109–125, 2005.

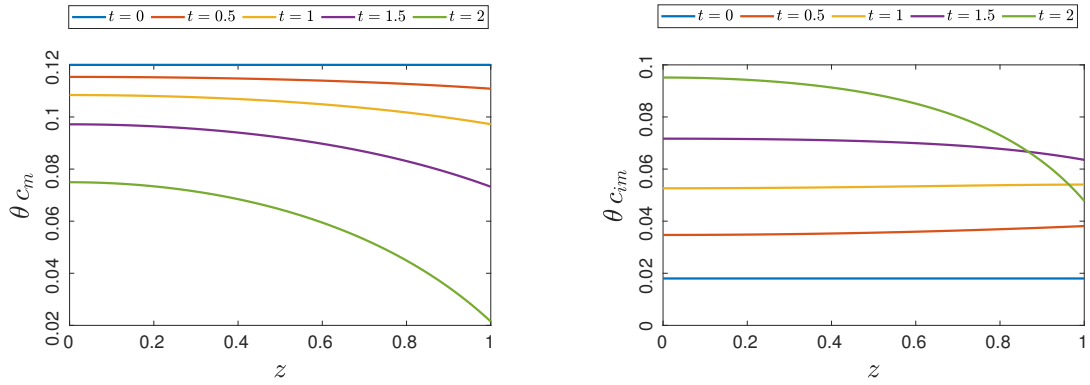

Figure 4: Evolution of monomer surfactant concentration for $R = 0.25$, $\theta_s = 0.6$, and $D = 8$ at times $t = 0$, $t = 0.5$, $t = 1$, $t = 1.5$, and $t = 2$ for (a) mobile species, and (b) immobile species.

Ternary Diagram Subgroup Report

Binan Gu, Jim Adriazola
New Jersey Institute of Technology

Valeria Barra
University of Colorado Boulder

Pak-Wing Fok
University of Delaware

Hilary and John Ockendon, Attila Kovacs, Maxim Zyskin
Oxford University

David Rumschitzki
City University of New York

and many more to thank

August 30, 2020

1 Introduction

In Gore's problem, there is a porous material that is filled with a liquid solution containing molecules from multiple species with known concentrations. As the solvent evaporates these molecules are left behind on the internal pore walls within the porous material. This subgroup in particular, was involved with the development of a mathematical model for the mass distribution of these molecular species within the porous material structure after all the solvent has evaporated completely given the porosity, pore size distribution, starting concentrations of species, and solution properties (density, viscosity, and surface tension). Ternary diagrams were chosen as the best tool to represent the modeling and evolution of the different species involved, in this case the solvent (water) and two surfactants.

1.1 Ternary Diagrams

A ternary diagram or ternary plot is a plot on three barycentric variables which sum to a constant, usually normalized to 1. It graphically depicts the ratios of the three variables as points on an equilateral triangle. It is used to show the compositions of systems composed of three species.

Figure 1 represents a simple ternary diagram. Suppose our three species are N_1, N_2 and N_3. The vertices marked A, B and C represent pure states, composed of all N_1, all N_2 and all N_3 respectively. Therefore, we may informally call A the N_1 vertex, B the N_2 vertex and C the N_3 vertex. A line parallel to one of the sides, and opposite a vertex indicates compositions which are constant with respect to the component represented by the vertex. On the other hand, when we travel along a line that is not parallel to any side of the triangle, or an arbitrary curve (see the green dotted line and blue curve, respectively, in Figure 2), none of the three components will be constant in general: see Figure 2 for some examples. In our problem, only planar, isothermal, ternary diagrams are of interest. More general ternary diagrams reflect temperature changes; a "temperature tower" representation in three dimensions is depicted in Figure 7 and discussed later in this report.

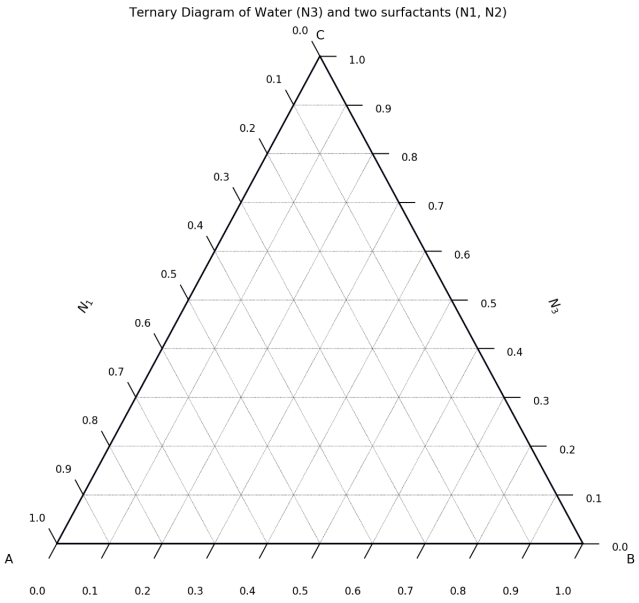

Figure 1: A simple ternary diagram. Vertex A is the "N_1 vertex" corresponding to states with all N_1 but no N_2, N_3. Vertex B is the N_2 vertex corresponding to states with all N_2 but no N_1, N_3. Vertex C is the N_3 vertex corresponding to states with all N_3 but no N_1, N_2.

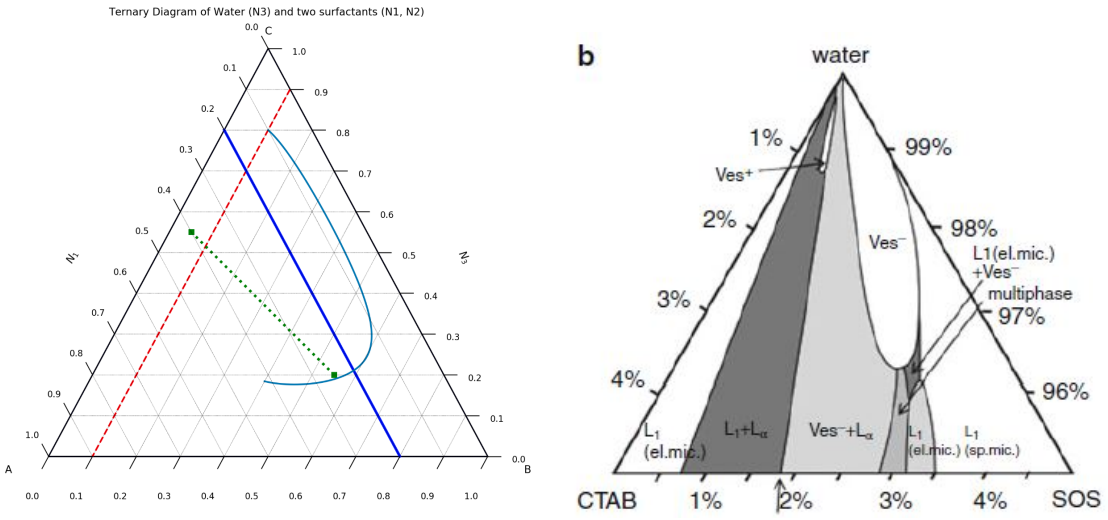

(a) (b)

Figure 2: (a) A simple ternary diagram with four trajectories representing evolving amounts of N_1, N_2 and N_3 such that $N_1 + N_2 + N_3 = 1$. For the dashed red line, N_2 is a constant and for the solid blue line, N_1 is a constant. (b) An empirical ternary diagram involving water, and two surfactants CTAB (cetrimonium bromide) and SOS (sodium octyl sulfate).

1.2 Basic Description of the Model

Let $N_1(t), N_2(t)$ and $N_3(t)$ be the mass of the two surfactants and water respectively (corresponding to surfactant A, B and water C in Figure 1). Let the total mass be

$$N(t) := N_1(t) + N_2(t) + N_3(t).$$

Define mass fraction as

$$\phi_i(t) = \frac{N_i(t)}{N(t)}, \quad i = 1, 2, 3.$$

The surface defined by $\phi_1 + \phi_2 + \phi_3 = 1$ forms a 2-simplex of length one. The triple (ϕ_1, ϕ_2, ϕ_3) (a point on the simplex) represents a specific composition of the three fluids. Our goal is to think of $\phi_k = \phi_k(t)$ as time-dependent variables and model the *dynamics* of each of the mass fractions, given an initial state $(\phi_1(0), \phi_2(0), \phi_3(0))$. We understand that $N_3(t)$ (water) decreases over time via evaporation at some given rate or governed by some evaporation law. Water leaves the system and the trajectory ends near the line AB in Figure 2, indicating that only the two surfactants are present by then, but as often happens, the problem is more complex than this intuition suggests.

We also attempt to capture the notion of the critical micelle concentration (CMC). This concentration corresponds to a critical mass fraction of surfactant in the solution mixture such that any concentration above this threshold triggers micelle formation from this particular surfactant. In our model, we have two different CMCs for the two surfactants.

2 A linear model

Assume $N_1(t), N_2(t), N_3(t) > 0$ for all $t \geq 0$. Suppose the mass of both surfactants does not change. Furthermore if we assume the concentration of surfactants is small, there is no micelle formation. Then we have the simple model

$$\frac{dN_1(t)}{dt} = 0, \quad N_1(0) = N_{1,0} \tag{1a}$$
$$\frac{dN_2(t)}{dt} = 0, \quad N_2(0) = N_{2,0} \tag{1b}$$
$$\frac{dN_3(t)}{dt} = -\alpha, \quad N_3(0) = N_{3,0} \tag{1c}$$

which has solutions

$$N_1(t) = N_{1,0} \tag{2a}$$
$$N_2(t) = N_{2,0} \tag{2b}$$
$$N_3(t) = N_{3,0} - \alpha t. \tag{2c}$$

given that $N_{1,0}, N_{2,0}$ are sufficiently small but positive. Hence,

$$N(t) = N_{1,0} + N_{2,0} + N_{3,0} - \alpha t. \tag{3}$$

Defining $N_0 = N_{1,0} + N_{2,0} + N_{3,0}$, the mass fractions are

$$\phi_1(t) = \frac{N_{1,0}}{N_0 - \alpha t} = \frac{\phi_1(0)}{1 - \beta t} \tag{4a}$$
$$\phi_2(t) = \frac{N_{2,0}}{N_0 - \alpha t} = \frac{\phi_2(0)}{1 - \beta t} \tag{4b}$$
$$\phi_3(t) = \frac{N_{3,0}}{N_0 - \alpha t} = 1 - \phi_1(t) - \phi_2(t), \tag{4c}$$

where $\beta = \frac{\alpha}{N_0}$ is the non-dimensional rate of evaporation. The mass fractions ϕ_k, $k = 1, 2, 3$ follow the ODEs

$$\frac{d\phi_1}{dt} = \alpha \frac{\phi_1}{N(t)} \tag{5a}$$
$$\frac{d\phi_2}{dt} = \alpha \frac{\phi_2}{N(t)} \tag{5b}$$
$$\frac{d\phi_3}{dt} = \alpha \frac{\phi_3}{N(t)} - \frac{\alpha}{N(t)}, \tag{5c}$$
$$\tag{5d}$$

where $N(t)$ is given by (3).

In a more realistic model, the solution mixture can undergo phase changes. For example, surfactants could form solid precipitates, or when the mass fraction of one of the surfactants reaches some critical level (not necessarily the same for each surfactant), they could form micelles. Assuming that N_1, N_2 are now amounts of non-micellar surfactant *in solution*, a direct modification to the ODEs could be the following (now dropping the low concentration restriction),

$$\frac{dN_1}{dt} = E_1(t) - D_1(t) - A_1(t), \quad N_1(0) = N_{1,0} \tag{6a}$$

$$\frac{dN_2}{dt} = E_2(t) - D_2(t) - A_2(t), \quad N_2(0) = N_{2,0} \tag{6b}$$

$$\frac{dN_3}{dt} = -\alpha, \quad N_3(0) = N_{3,0} \tag{6c}$$

$$\frac{dN_{\text{mic}}}{dt} = E_{\text{mic}}(t), \quad N_{\text{mic}}(0) = 0, \tag{6d}$$

where $E_i(t)$ is the evolution law for surfactant i after the CMC has been reached; A_1, A_2 are the adsorption rates of the surfactants to the sides of the pores; and D_1, D_2 are the rates at which the surfactants form a solid precipitate. In the following analysis, we assume $A_1 = A_2 = D_1 = D_2 = 0$.

Let $\Theta(x)$ be the Heaviside step function so $\Theta(x) = 1$ when $x > 0$ and $\Theta(x) = 0$ when $x \leq 0$. Then the reaction rate, $E_1(t), E_2(t)$ can be determined from mass action kinetics:

$$E_1(t) = \left(\underbrace{-n_1 k_+ N_1^{n_1}}_{\text{Micelle Formation}} + \underbrace{n_1 k_- N_{\text{mic}}}_{\text{Micelle Dissociation}} \right) \Theta(\phi_1 - \phi_{1,\text{crit}}) \tag{7a}$$

$$E_2(t) = \left(\underbrace{-n_2 k_+ N_2^{n_2}}_{\text{Micelle Formation}} + \underbrace{n_2 k_- N_{\text{mic}}}_{\text{Micelle Dissociation}} \right) \Theta(\phi_2 - \phi_{2,\text{crit}}) \tag{7b}$$

$$E_{\text{mic}}(t) = \underbrace{-\left(\sum_{i=1}^{2} \Theta(\phi_i - \phi_{i,\text{crit}}) \right) k_- N_{\text{mic}}}_{\text{Micelle Dissociation}} + \underbrace{k_+ N_1^{n_1} \Theta(\phi_1 - \phi_{1,\text{crit}}) + k_+ N_2^{n_2} \Theta(\phi_2 - \phi_{2,\text{crit}})}_{\text{Micelle Formation}} \tag{7c}$$

where n_i's are the order of the reaction for the micelle formation of each surfactant respectively and $\phi_i = N_i/(N_1 + N_2 + N_3)$ as before. To maintain model tractability, we do not distinguish between micelles formed by the two surfactants. Therefore, as long as one surfactant reaches its CMC, micelle formation commences; this is reflected in the summation term on the Heaviside function involving the mass fraction of each surfactant in eq. (7c), $\sum_{i=1}^{2} \Theta(\phi_i - \phi_{i,\text{crit}})$. The dissociation rate of the micelles is captured by the first term in eq. (7c). The accretion rate of the micelles is represented by the second and third terms, which describe the contribution to micelle formation from either surfactant, providing it reaches its CMC. Altogether, we see that the rates of change of all three species follow detailed balance.

Note that $\phi_{1,\text{crit}}$ and $\phi_{2,\text{crit}}$ are two separate input parameters to the problem, but they can potentially be related. A deeper analysis based on chemical potential can be used to derive the rate terms E_1 and E_2.

3 Results

In this section, we discuss some preliminary results that rely on the solution of the system of ODEs in eqs. (6) and the evolution rate functions in eqs. (7). The ODEs (6) are solved subject to the initial conditions

$$N_1(0) = N_{1,0}, \tag{8a}$$
$$N_2(0) = N_{2,0}, \tag{8b}$$
$$N_3(0) = N_{3,0}, \tag{8c}$$
$$N_{\text{mic}}(0) = 0. \tag{8d}$$

In the following discussion, our results abide by the following assumptions. Firstly, we do not distinguish between the micelle production rate k_- between the two surfactants. Secondly, the moment micelle production begins, *i.e.*, when at least one surfactant reaches its CMC, micelles dissociate at a constant rate k_+. Lastly, the order of reaction for each surfactant is kept equal (except in figure 6).

In figure 3(a), we present the evolution of mass fraction of each species in the solution mix with a given initial condition on the mass fractions, and a reaction order of 1 (so $n_1 = n_2 = 1$). At the early stage of the evolution, water takes up the majority of total mass while concentrations of the surfactants increase over time as water evaporates. The Heaviside triggers, *i.e.*, the arrival at the CMC of either surfactant, correspond to dN_{mic}/dt changing from 0 to > 0. The surfactants mass fractions eventually taper off to reach an equilibrium while water has completely evaporated.

When the order of the reaction is increased to 3 (see figure 3(b)), the Heaviside triggers are more pronounced, exemplified by the kinks in the evolution curves of the mass fractions of the two surfactants (*e.g.*, surfactant 2, near $(\text{time}, \phi_2) = (1, 0.15)$). Another kink (barely visible from the blue curve for surfactant 1) near $t = 1.5$ for surfactant 1 is also present when its mass fraction reaches CMC at $\phi_2 = 0.1$. Micelle formation occurs also more quickly which eventually causes the surfactants to occupy less (and decreasing) mass fractions.

To visualise the evolutions of the species (water, surfactants 1 and 2) on a ternary diagram, we plot their trajectories in figure 4 with various initial conditions and a fixed reaction order of 1. Since mass fraction of water (vertical axis) is always decreasing due to evaporation, a typical trajectory on the simplex will always travel "down" the plane, *i.e.*, in a direction with negative vertical component, from any initial conditions except the ones with $N_3(0)$. Numerically, we observe that the evolution of the mass ratio $N_1(t)/N_2(t)$ of the two surfactants remain close to the initial value $N_1(0)/N_2(0)$ when $n_1 = n_2 = 1$, corresponding to straight trajectories in the ternary diagram.

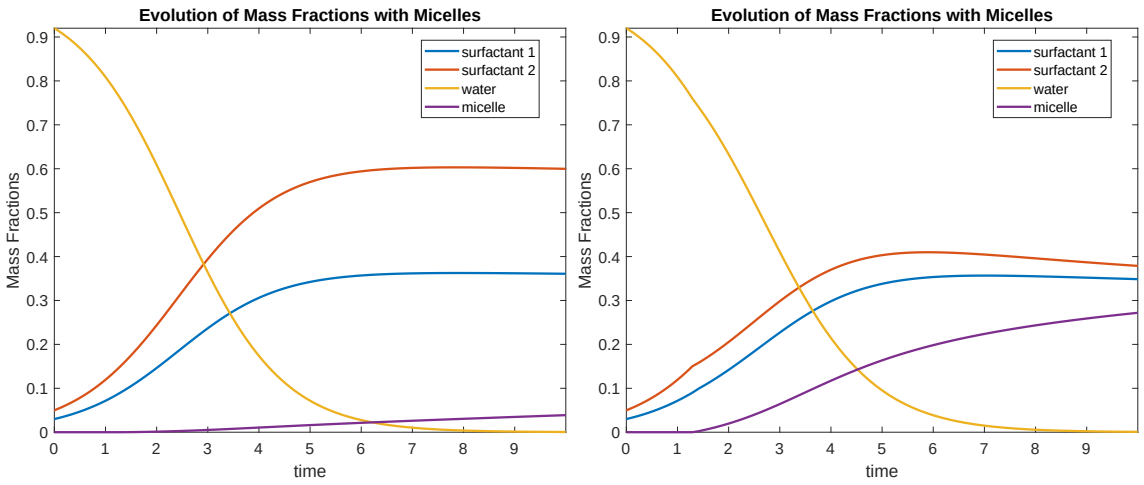

(a) (b)

Figure 3: mass fractions evolution according to eqs. (6) with fixed parameters $\alpha = 1$, $k_- = 0.01$, $k_+ = 0.005$, $N_{\text{mic}}(0) = 0$, $\phi_{1,\text{crit}} = 0.1$ and $\phi_{2,\text{crit}} = 0.15$. Initial conditions are $N_{1,0} = 3$, $N_{2,0} = 5$. Reaction orders are (a) $n_1 = n_2 = 1$; (b) $n_1 = n_2 = 3$.

In figure 5, we consider different reaction orders as chemical reagents such as surfactants may possess vastly different chemical characteristics. The trajectory in blue is formed by exactly the same parameter chosen in figure 4 for the same color. However, the trajectories in red and black use a reaction of order 1 for surfactant 1, but order 2 and 3 respectively for surfactant 2. The kink in the black curve (corresponding to a high reaction order) showcases the start of micelle production and a completely different trajectory than the other two. Especially towards the exhaustion of water near the bottom of the simplex, in the black and red curves, the sharp turn towards $(1, 0, 0)$ (corresponding to a pure state of surfactant 1) indicates that surfactant 1 begins to occupy larger mass fractions. This is because surfactant 2 with its larger reaction order produces micelles and hence loses mass more quickly. We also see that this effect is triggered earlier in the black curve when the reaction order of surfactant 2 is further increased to $n_2 = 3$.

In figure 6, we investigate the regime where the two surfactants have a relatively large initial difference in mass fractions. We still vary only the reaction order of the second surfactant similar to figure 4. Note that the CMC for the surfactant with larger initial mass fraction is set much higher because we wish to visualise its evolution (or otherwise it is always producing micelles). We see that the "kinks" in the curve (due to the onset of micelle formation) are more pronounced when the reaction order is high (black curve with $n_2 = 3$), resembling the kinks in figure 3b (but with different initial conditions and CMCs). Furthermore, the dynamics past the kink in the black curve exhibits first a quicker decrease in mass fraction of surfactant 2 than the red and blue counterparts. Then it settles into a relative equilibrium as micelle production and surfactant mass loss balance out while only water evaporation is taking place. When water mass fraction is close to zero near the bottom

of the simplex, we see a similar effect as in figure 4 where the mass fraction of surfactant 1 increases due to the rapid loss surfactant 2 due to rapid micelle formation.

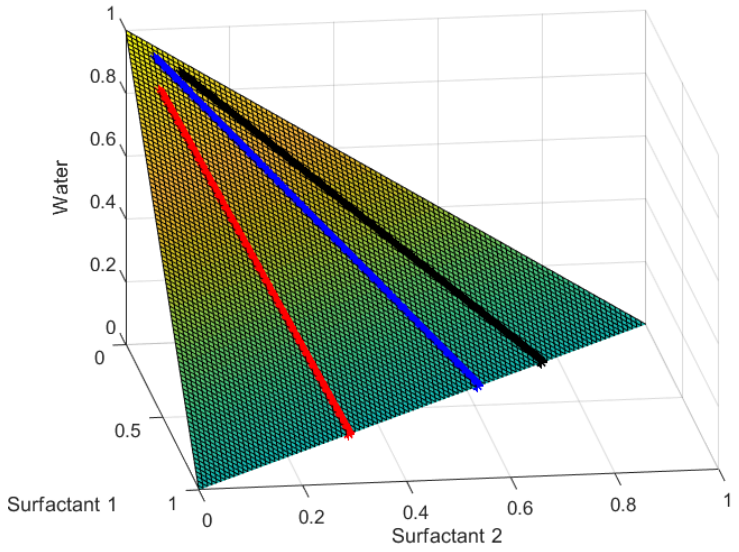

Figure 4: Trajectories of mass fractions of water, surfactant 1 and 2 according to eqs. (6) and eqs. (7) with fixed parameters $\alpha = 1$, $k_- = 0.01$, $k_+ = 0.005$, $N_{\text{mic}}(0) = 0$, $\phi_{1,\text{crit}} = 0.1$ and $\phi_{2,\text{crit}} = 0.15$. Reaction orders are $n_1 = n_2 = 1$. Total mass is kept at a constant $N = N_{1,0} + N_{2,0} + N_{3,0} = 100$. Initial conditions of the three species are: (red) $N_{1,0} = 10$, $N_{2,0} = 5$; (blue) $N_{1,0} = 3$, $N_{2,0} = 5$; (black) $N_{1,0} = 3$, $N_{2,0} = 10$.

4 Future work

Although Gore's suggestion was to devise a model for constant temperature, one of the references provided [1] discussed the notion of a critical micelle temperature (CMT). Depending on whether the temperature is below or above the CMT, our model for mass fraction evolution could be different. Taken together, the CMT and CMC can result in very complicated evolutions of the system. For the non-isothermal case, we may have mass fractions that change with respect to temperature, so that $\phi_k = \phi_k(T, t)$ reflected by the inclusion of a temperature axis in the ternary diagram: see figure 7. However, our current model does not include the influence of ambient temperature.

Lastly, one may also consider a variational approach, such that the time-evolution of the path on the simplex surface is described by some energy minimizing curve, along with constraints imposed by the CMT or CMC. This aspect could be explored in future endeavors.

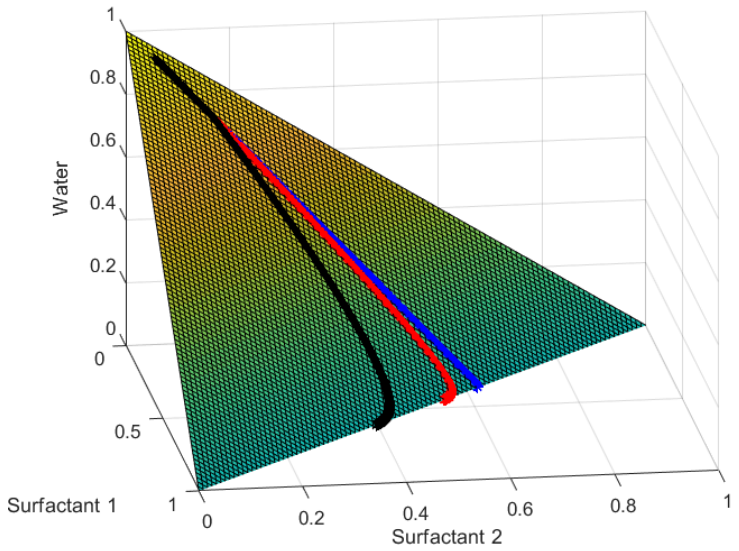

Figure 5: Trajectories of mass fractions of water, surfactant 1 and 2 according to eqs. (6) and eqs. (7) with fixed parameters $\alpha = 1$, $k_- = 0.01$, $k_+ = 0.005$, $N_{\text{mic}}(0) = 0$, $\phi_{1,\text{crit}} = 0.1$ and $\phi_{2,\text{crit}} = 0.15$. Initial conditions are fixed at $N_{1,0} = 3$, $N_{2,0} = 5$. Reaction orders are: $n_1 = 1$, $n_2 = 1$ (blue); $n_1 = 1$, $n_2 = 2$ (red); and $n_1 = 1$, $n_2 = 3$ (black).

References

[1] Hammouda, B.: Phase diagrams for micellar systems. URL https://www.ncnr.nist.gov/staff/hammouda/summer_school_2/chapter_42.pdf

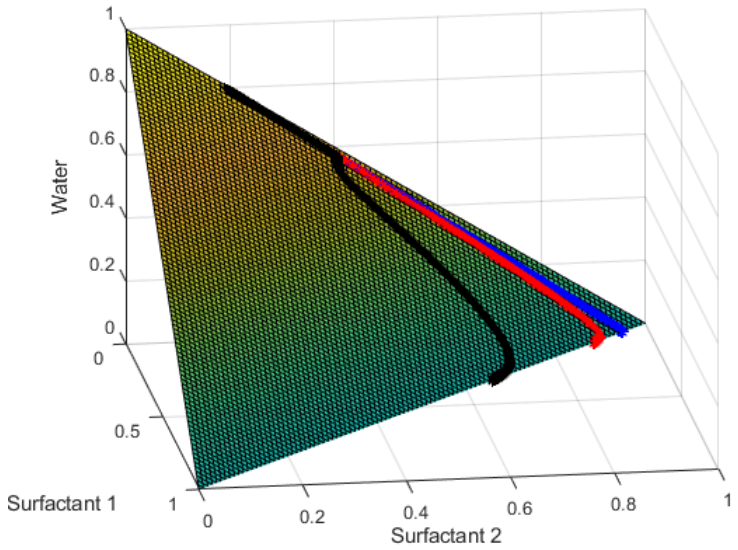

Figure 6: Trajectories of mass fractions of water, surfactant 1 and 2 according to eqs. (6) and eqs. (7) with fixed parameters $\alpha = 1$, $k_{-} = 0.01$, $k_{+} = 0.005$, $N_{\mathrm{mic}}(0) = 0$, $\phi_{1,\mathrm{crit}} = 0.15$ and $\phi_{2,\mathrm{crit}} = 0.4$. Initial conditions are fixed at $N_{1,0} = 1$, $N_{2,0} = 19$. Reaction orders are: $n_1 = 1$, $n_2 = 1$ (blue); $n_1 = 1$, $n_2 = 2$ (red); and $n_1 = 1$, $n_2 = 3$ (black).

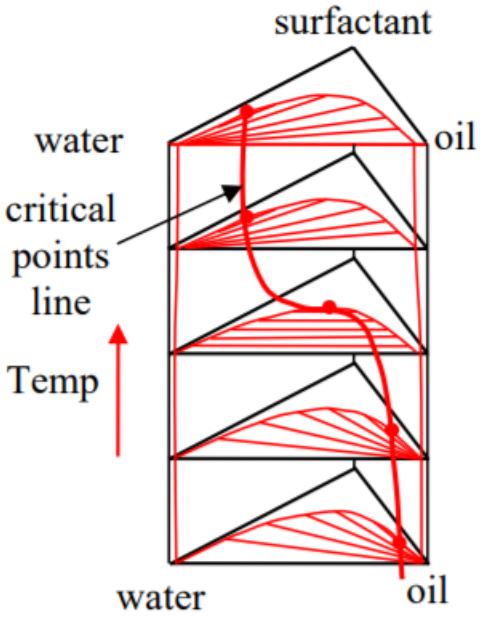

Figure 7: Temperature Tower: at each level of the temperature, the "parabolic" red curve separates the phases. The red straight lines are tie lines, such that linear combinations of any two points (two possible choices of mixture compositions) on those stay in the same phase. Otherwise, the mixture does not mix (in the white region). For each temperature, there may (or may not in theory) exist a critical point (plait point) such that any perturbation (in composition, or in temperature) to it will lead to a phase transition. We can track the plait point for every temperature level to form a critical points line, climbing up the "hypersurface" as temperature increases. Eventually, we will reach a temperature so high that all fluids become gaseous and thus reach a 1-phase indefinitely unless the temperature drops.